NOGAPS-ALPHA model simulations of stratospheric ozone during the SOLVE2 campaign

J. P. Mccormack, S. D. Eckermann, L. Coy, D. R. Allen, Y.-J. Kim, T. Hogan, B. Lawrence, A. Stephens, E. V. Browell, J. Burris, et al.

Atmos. Chem. Phys. Discuss., 4, 4227–4284, 2004
www.atmos-chem-phys.org/acpd/4/4227/
SRef-ID: 1680-7375/acpd/2004-4-4227

Atmospheric Chemistry and Physics Discussions

NOGAPS-ALPHA model simulations of stratospheric ozone during the SOLVE2 campaign

J. P. McCormack[1], S. D. Eckermann[1], L. Coy[1], D. R. Allen[2], Y.-J. Kim[3], T. Hogan[3], B. Lawrence[4], A. Stephens[4], E. V. Browell[5], J. Burris[6], T. McGee[6], and C. R. Trepte[5]

[1]E.O. Hulburt Center for Space Research, Naval Research Laboratory, Washington DC, USA
[2]Remote Sensing Division, Naval Research Laboratory, Washington DC, USA
[3]Marine Meteorology Division, Naval Research Laboratory, Monterey, California, USA
[4]British Atmospheric Data Center, Rutherford Appleton Laboratory, Oxfordshire, UK
[5]NASA Langley Research Center, Hampton, Virginia, USA
[6]NASA Goddard Space Flight Center, Greenbelt, Maryland, USA

Received: 17 June 2004 – Accepted: 9 July 2004 – Published: 4 August 2004

Correspondence to: J. P. McCormack (mccormack@nrl.navy.mil)

Abstract

This paper presents three-dimensional prognostic ozone simulations with parameterized photochemistry from the new NOGAPS-ALPHA middle atmosphere forecast model. We compare 5-day NOGAPS-ALPHA hindcasts of stratospheric ozone with a combination of satellite and DC-8 aircraft measurements for two specific cases during the SOLVE II campaign: (1) the cold, isolated vortex during 11–16 January 2003; and (2) the rapidly developing stratospheric warming of 17–22 January 2003. In the first case we test three different photochemistry parameterizations. NOGAPS-ALPHA ozone simulations using the NRL-CHEM2D parameterization give the best overall agreement with SAGE III and POAM III profile measurements. 5-day NOGAPS-ALPHA hindcasts of polar ozone initialized with the NASA GEOS4 ozone analyses produce better agreement with observations than do the operational ECMWF ozone forecasts. In the second case, comparisons between NOGAPS-ALPHA and ECMWF 114-h forecasts of the split vortex structure in stratospheric ozone on 21 January 2003 show comparable skill. Updated ECMWF ozone forecasts of this case at hour 42 display marked improvement from the 114-h forecast; corresponding updated 42-h NOGAPS-ALPHA prognostic ozone simulations do not improve significantly. In general, these results demonstrate that the spectral advection component in NOGAPS-ALPHA is well-suited for middle atmosphere tracer transport. In particular, we find that stratospheric ozone forecasts at high latitudes in winter can depend on both model initial conditions and the treatment of photochemistry even over a period of 5 days.

1. Introduction

The Navy Operational Global Atmospheric Prediction System (NOGAPS) is the US Department of Defense's (DoD's) high-resolution global numerical weather prediction (NWP) system, run operationally at the Navy's Fleet Numerical Meteorology and Oceanography Center (FNMOC). NOGAPS is a complete NWP system that includes

ACPD

4, 4227–4284, 2004

data quality control (Baker, 1992), tropical cyclone bogusing (Goerss and Jeffries, 1994), operational data assimilation (Goerss and Phoebus, 1992; Daley and Barker, 2001), nonlinear normal mode initialization (Errico et al., 1988), and a global spectral forecast model (Hogan and Rosmond, 1991; Hogan et al., 1991). NOGAPS forecasts are distributed to numerous defense and civilian users for input to environmental prediction systems such as FNMOC's ocean wave, sea ice, ocean thermodynamics, and tropical cyclone models.

NOGAPS forecasts also support various aircraft and ship-routing programs, a capability that was utilized during NASA's second SAGE III Ozone Loss and Validation Experiment (SOLVE2), from January–February 2003. The first two authors used NOGAPS forecasts in the field as part of the Naval Research Laboratory's (NRL) in-field flight-planning support for NASA's instrumented DC-8 research aircraft. Specific applications included forecasting anticyclonic "minihole" systems whose synoptic uplift and adiabatic cooling might form polar stratospheric clouds (PSCs) (McCormack and Hood, 1997), and initialization of other NRL models that predicted in-flight mountain wave turbulence for the DC-8 and areas of possible mountain wave PSC formation (Eckermann et al., 2004a). These forecasts played important roles in devising scientifically valuable DC-8 flights during SOLVE2, such as the 4 February 2003 flight that measured mountain wave PSCs within an evolving minihole event over Iceland.

Despite these stratospheric applications during SOLVE2, operational NOGAPS forecasts currently focus primarily on the troposphere. As part of a major initiative to improve its NWP and data assimilation capabilities, a new prototype version of the NOGAPS global-spectral circulation model (GCM) has been developed over the past several years (Eckermann et al., 2004b) which extends the model through the stratosphere and into the mesosphere. This new Advanced Level Physics-High Altitude (ALPHA) version of the NOGAPS GCM is described in Sect. 2.

One major focus of development in NOGAPS-ALPHA has been to add ozone to the GCM as a fully interactive three-dimensional prognostic variable. The addition of prognostic ozone is a necessary first step toward the goal of operationally as-

ACPD
4, 4227–4284, 2004

similating and forecasting ozone fields using NOGAPS. This development supports concurrent efforts to operationally assimilate satellite radiances directly using NRL's new Atmospheric Variational Data Assimilation System (NAVDAS) (Daley and Barker, 2001; Goerss et al., 2003), potentially improving overall NWP performance in several ways. For example, prognostic ozone can help correct complex biases in some long-wave radiance channels due to ozone absorption (Derber and Wu, 1998). Prognostic ozone fields, when fed into the radiation calculations, should also improve stratospheric heating/cooling rates and surface radiation fluxes. Operational assimilation of satellite ozone data into NOGAPS may also add valuable meteorological information that can aid overall forecast skill (Jang et al., 2003). These types of issues have motivated ozone assimilation and forecasting efforts at other operational centers, such as the National Centers for Environmental Prediction (NCEP), the European Center for Medium Range Weather Forecasts (ECMWF), and NASA's Global Modeling and Assimilation Office (GMAO).

The combination of ozone and ozone-related observations from a variety of satellite and airborne instruments makes the SOLVE2 winter an ideal period for running NOGAPS-ALPHA in hindcast mode to test the performance of our new initialization, advection and photochemistry algorithms for ozone. This is the primary focus of the present work. In addition to conducting comparisons with satellite and aircraft ozone measurements, we also compare our NOGAPS-ALPHA ozone fields with ozone forecasts and analyses issued operationally by the ECMWF and with the NASA GEOS4 ozone analyses.

It is particularly interesting to assess the performance of current NWP ozone analysis/forecast methods within the context of the SOLVE2 mission. For NWP systems, cost-benefit considerations do not currently justify the use of the detailed multi-reaction chemistry and photolysis schemes for ozone currently used in some state-of-the-art climate-chemistry models and offline chemical transport models (CTMs). Thus, in common with other NWP models like ECMWF and NCEP's Global Forecasting System (GFS), NOGAPS-ALPHA uses much simpler (and faster) linearized ozone photochem-

ACPD
4, 4227–4284, 2004

istry schemes that efficiently parameterize the major homogeneous photochemical dependences. The accuracy of these parameterizations in real meteorological situations is not clear, and ozone forecasts issued by NWP models using these schemes have not been subjected to detailed comparisons with data to answer these questions experimentally.

The SOLVE2 case studies in this paper provide initial validation assessments of NOGAPS-ALPHA prognostic ozone using parameterized photochemistry schemes. These assessments will guide future NWP model development. For example, the potential for heterogeneous ozone loss in the Arctic is highly sensitive to the synoptic meteorological conditions. This process only becomes important if the vortex is stable and thus cold. Within the linearized ozone photochemistry framework, heterogeneous reactions producing catalytic ozone losses can be parameterized using, e.g. an additional chlorine loading term (Dethof, 2003), or using a so-called cold-tracer scheme (Braesicke et al., 2003). Whether or not such developments are justified depends on the impact of the omitted effects on NWP skill relative to the requisite computational overhead. The combination of the basic linearized gas phase ozone photochemistry parameterizations and NWP model's internal transport algorithms must be able to capture observed features in the polar ozone distribution (e.g. ozone lamination due to vortex filaments) before additional heterogeneous terms can then potentially yield an improved ozone forecast. This paper presents first-order assessments of these parameterizations for select cases during the SOLVE II campaign.

The meteorological conditions during the SOLVE2 winter period allow us to study the performance of NOGAPS-ALPHA prognostic ozone fields under both relatively quiescent and disturbed polar vortex conditions. From early December 2002 to mid-January 2003, the Arctic polar vortex was relatively stable and lower stratospheric temperatures were cold enough to form PSCs. A stratospheric warming beginning on or around 17 January 2003 caused the vortex to split into two distinct lobes by 21 January (Urban et al., 2004). Figure 1 depicts the rapid change in 30 hPa minimum temperatures over the Northern polar region during January 2003.

ACPD
4, 4227–4284, 2004

This paper presents results from NOGAPS-ALPHA hindcast runs (with prognostic ozone activated) that span these two distinctly different periods in January 2003. Case 1 (see Fig. 1) corresponds nominally to the DC-8 flight of 14 January 2000, during the period of cold, relatively undisturbed vortex conditions that existed during 11–16 January. Our NOGAPS-ALPHA forecasts are initialized on 11 January and run throughout this 5-day period. Our comparisons here focus on the full ozone profile throughout the stratosphere, and thus we compare mostly with satellite data since DC-8 ozone profiles do not extend quite as high. Case 2 focuses on the DC-8 flight on 21 January, toward the end period of the rapid initial warming of the stratosphere and splitting of the vortex during 17–22 January. The complex meteorology of this event is used as a stern test of NOGAPS-ALPHA model dynamics and transport. For this case, we compare more closely with DC-8 lidar data along a flight track at heights ∼13–30 km. At these altitudes ozone photochemical relaxation times at all latitudes are fairly long, and thus transport effects should dominate. These case studies are the first assessments of NOGAPS-ALPHA model performance.

The paper is organized as follows: Sect. 2 provides a description of the major modifications of the NOGAPS-ALPHA GCM compared to the current operational NOGAPS; Sect. 3 gives an overview of the various data sources used to validate the NOGAPS-ALPHA simulations; Sect. 4 focuses on the period of 11–16 January 2003, presenting an intercomparison of 3 different ozone photochemistry schemes in NOGAPS-ALPHA validated with a combination of SAGE III and POAM III ozone profile measurements; Sect. 5 presents an assessment of NOGAPS-ALPHA prognostic ozone during the rapidly developing stratospheric warming during the period 17–22 January 2003; Sect. 6 summarizes these results and outlines future research.

ACPD
4, 4227–4284, 2004

2. Model description

2.1. Overview

The operational NOGAPS GCM is a spectral model with triangular truncation at zonal and meridional wavenumber 239 ("T239", roughly equivalent to 0.5° latitude/longitude spacing). It utilizes a generalized vertical coordinate within an energy conserving vertical finite difference formulation (Kasahara, 1974; Simmons and Burridge, 1981; Hogan and Rosmond, 1991). The model's dynamical variables are relative vorticity, divergence, virtual potential temperature, specific humidity, and surface pressure. The model is central in time with a semi-implicit treatment of gravity wave propagation and Robert time filtering (Simmons et al., 1978). The current NOGAPS-ALPHA model's physics packages include a bulk Richardson number-dependent vertical mixing scheme (Louis et al., 1982), a time-implicit Louis surface flux parameterization (Louis, 1979), orographic gravity wave drag (Webster et al., 2003), shallow cumulus mixing of moisture, temperature, and winds (Tiedtke, 1984), the Emanuel cumulus parameterization (Emanuel and Zivkovic-Rothman, 1999), convective and stratiform cloud parameterizations (Teixeira and Hogan, 2002), and radiative heating and cooling based on Harshvardhan et al. (1987).

2.2. NOGAPS-ALPHA vertical coordinate

Designed primarily for tropospheric applications, the operational NOGAPS model has a vertical domain extending from the surface to 1 hPa (~48 km altitude) and lacks any representation of middle atmospheric gravity wave drag. Figure 2a illustrates the operational model's vertical levels at one particular latitude. In this configuration, unrealistically large numerical diffusion is applied over a broad region of the model's upper vertical domain (1–20 hPa). This broad "sponge layer" limits the uppermost vertical level where operational NOGAPS output can be used to 30 hPa (~26 km). The lack of middle atmospheric gravity wave drag promotes an extreme cold bias in wintertime

ACPD
4, 4227–4284, 2004

polar temperatures. Operational NOGAPS stratospheric temperature forecasts were systematically 4–5 K too cold within the Arctic polar vortex during SOLVE2, preventing accurate quantitative predictions of PSC formation.

To improve middle atmosphere simulations (e.g. Trenberth and Stepaniak, 2002), NOGAPS-ALPHA replaces the current terrain-following vertical coordinate ("σ") with a hybrid "σ-p" vertical grid that transitions from terrain-following near the surface to pure pressure levels at 85 hPa. Figure 2b demonstrates how this new formulation smoothly transitions to constant pressure height thicknesses in the stratosphere over arbitrary topography. This uniform vertical resolution is similar to current choices adopted at ECMWF and offers better resolved middle atmosphere dynamics; in particular, better simulations of explicitly-generated gravity waves throughout the entire depth of the atmosphere.

2.3. Radiative heating

Raising the top boundary of the NOGAPS-ALPHA model requires an improved treatment of middle atmospheric radiative heating. To this end, we have replaced the operational model's current radiative heating scheme (Harshvardhan et al., 1987) with the CLIRAD longwave (Chou et al., 2001) and shortwave (Chou and Suarez, 2002) schemes, improving the net heating calculations at all levels but particularly in the middle atmosphere. Specifically, the updated CLIRAD shortwave heating rates include contributions from O_2 and near-infrared CO_2 bands that are not contained in the operational radiative heating scheme. Neglecting these contributions can result in underestimating the peak shortwave heating in the middle atmosphere by as much as 1–2 K day^{-1}.

Shortwave heating and longwave cooling rates are currently computed using two-dimensional (height-latitude) climatological tables of ozone and water vapor mixing ratios. For NOGAPS-ALPHA, these tables have been updated using the monthly mean ozone climatology of Fortuin and Kelder (1998) (1000–0.3 hPa) and HALOE water vapor measurements from 100–0.3 hPa (Pumphrey et al., 1998). Above the 0.3 hPa level,

the ozone and water vapor values are based on long-term climate output from NRL's CHEM2D model (McCormack and Siskind, 2002).

2.4. Gravity wave drag

As with all global models that extend through the stratosphere and mesosphere, considerable attention must be paid to the parameterization of gravity wave drag (GWD) to yield a realistic mesospheric circulation. To this end, we have coded and implemented within NOGAPS-ALPHA four GWD schemes. These four schemes consist of two spectral GWD schemes for the middle atmosphere (Hines, 1997; Alexander and Dunkerton, 1999), a new orographic GWD scheme (Kim, 1996) based on the work of Kim and Arakawa (1995), and a cloud/convection-generated GWD scheme based on Chun and Baik (2002). The performance of these schemes in NOGAPS-ALPHA has not yet been rigorously tested. Therefore, the model calculations presented here utilize two different Rayleigh friction profiles applied to the zonal winds above ~40 km (see Fig. 3). The first profile is a modification of the profile used by Lin and Williamson (2000) and imposes very strong drag on the zonal winds in the upper stratosphere and mesosphere. The second profile, based on the standard profile of Butchart and Austin (1998), imposes less drag on the zonal winds, and is more representative of values commonly used in many global NWP models. Unless noted otherwise, all NOGAPS-ALPHA simulations presented here use the standard profile of Butchart and Austin (1998). In the troposphere, NOGAPS-ALPHA currently uses orographic gravity wave drag computed using the method of Palmer et al. (1986).

Although the use of Rayleigh friction is a crude proxy for mesospheric GWD that can reduce realistic middle atmospheric variability (e.g. Shepherd et al., 1996; Lawrence, 1997), it's performance has been documented in previous global NWP and climate models (see, e.g. Shepherd et al., 1996; Butchart and Austin, 1998; Pawson et al., 1998). We have tested this mesospheric Rayleigh friction in a 5-year free-running simulation of an earlier low horizontal resolution T79L54 version of NOGAPS-ALPHA using the Rayleigh friction profile of Boville (1986). Figure 4 plots monthly averaged

zonal-mean zonal winds for January, April, July, and October, which show reasonable agreement with climatological values (e.g. Randel et al., 2002). Figure 5 plots the mean meridional circulation computed as a mass flux from the residual mean mass stream function for January, April, July, and October. We see that, despite being designed primarily for short-term NWP, the NOGAPS-ALPHA middle atmosphere reproduces a realistic climatological Brewer-Dobson stratospheric circulation and a clear pole-to-pole mesospheric residual circulation. Quantitative analysis of the strength of the residual mean meridional circulation in NOGAPS-ALPHA are currently underway.

2.5. Upper level initialization

The NOGAPS-ALPHA model is initialized using combined output from the Multi-Variate Optimal Interpolation (MVOI) system up to 10 hPa (Goerss and Phoebus, 1992) and an experimental "STRATOI" product based on TOVS radiances that provides winds and temperatures up to 0.4 hPa. Above 0.4 hPa, NOGAPS-ALPHA extrapolates the top-most initialization wind, temperature and geopotential fields by progressively relaxing them with increasing altitude to climatological values from the CIRA 1986 reference atmosphere (Fleming et al., 1990). Given the unreliability of mesospheric CIRA winds during certain months, particularly near the equator (Randel et al., 2002), we have created an additional option of choosing climatological wind fields from the UARS Reference Atmosphere Project (Swinbank and Ortland, 2003) for this upper-level initialization. In late 2003, initialization of the operational NOGAPS model transitioned from MVOI to the NRL Variational Data Assimilation System (NAVDAS) up to 10 hPa (Daley and Barker, 2001; Goerss et al., 2003). This system is designed to include the direct assimilation of satellite radiances, providing the motivation for development of a prognostic ozone scheme in NOGAPS-ALPHA.

ACPD
4, 4227–4284, 2004

2.6. Prognostic ozone

An important goal of the NOGAPS-ALPHA development project is to improve operational assimilation of satellite radiance measurements. This requires a detailed description of atmospheric radiative absorption and emission. To meet this goal, a new three-dimensional (3-D) prognostic ozone scheme has been implemented in NOGAPS-ALPHA. Two separate model constituents are initialized with 3-D ozone mixing ratios from the GMAO Global Earth Observation System (GEOS) ozone data assimilation system (Stajner et al., 2001). The first constituent represents "passive" ozone, where the constituent is only subject to advection as calculated by the model's spectral transport scheme. The second constituent represents "active" ozone, which is subject to both advection and photochemical production and loss. The passive ozone tracer is a powerful tool for diagnosing model transport in the middle atmosphere. By taking the difference between active and passive ozone, one can distinguish between dynamical and photochemical variations in ozone.

Once initialized, NOGAPS-ALPHA prognostic chemical fields are transported globally using the same spectral method used to advect meteorological variables such as vorticity and specific humidity within the GCM. It is well-known that, over time, spectral advection yields fine-scale "noise" in model advected fields (Rasch et al., 1990; Fairlie et al., 1994). We suppress this effect in NOGAPS-ALPHA prognostic chemical fields by applying a small amount of ∇^4 horizontal spectral diffusion after each time step, with a diffusion coefficient of equal magnitude to that applied to the meteorological divergence fields. For the runs reported here, this was applied to the isobaric stratospheric layers only.

Since NOGAPS-ALPHA is primarily a forecast model, calculating the ozone production and loss terms for the active ozone field using full photochemistry is too computationally expensive. Instead, the net ozone photochemical production/loss rate ($P-L$) can be approximated with a linear function of three model variables: the local ozone mixing ratio (r), temperature (T), and overlying ozone column abundance (Σ), (Cariolle

ACPD
4, 4227–4284, 2004

and Deque, 1986; McLinden et al., 2000). The functional form of the ozone photochemical tendency equation can then be expressed as:

$$\frac{\partial r}{\partial t} = (P-L)_o + \frac{\partial (P-L)}{\partial r}[r - r_o] + \frac{\partial (P-L)}{\partial T}[T - T_o] + \frac{\partial (P-L)}{\partial \Sigma}[\Sigma - \Sigma_o] \quad (1)$$

where the coefficients $(P-L)_o$, $\frac{\partial (P-L)}{\partial r}$, $\frac{\partial (P-L)}{\partial T}$, and $\frac{\partial (P-L)}{\partial \Sigma}$ represent diurnally averaged quantities that are computed offline with a complete 2-D (altitude-latitude) photochemical model. The term $(P-L)_o$ is the net ozone mixing production/loss term (in ppmv s^{-1}) evaluated at photochemical equilibrium. The quantities r_o, T_o, and Σ_o refer to the ozone mixing ratio, temperature, and column abundance at photochemical equilibrium. In practice, however, r_o is replaced with the 2-D climatological values of Fortuin and Kelder (1998), consistent with the ozone photochemistry parameterization in the ECMWF model (Dethof and Holm, 2002). Currently NOGAPS-ALPHA applies the photochemistry scheme up to 1 hPa, then smoothly relaxes to 2-D climatological ozone mixing ratios in the mesosphere. This is in keeping with the linear assumptions on which Eq. (1) is based, which break down in the upper stratosphere and mesosphere.

Section 4 compares results from three different linearized photochemistry parameterizations in order to determine the sensitivity of the prognostic ozone simulations to the details of the parameterization. Specifically, we compare NOGAPS-ALPHA "active" ozone fields computed using the Cariolle and Deque (1986) coefficients (hereafter CD86), the McLinden et al. (2000) coefficients (hereafter LINOZ), and the CHEM2D coefficients. Note that the CHEM2D scheme currently employs only the first two terms on the right hand side of Eq. (1), representing the mean production/loss $(P-L)_o$ and sensitivity to local ozone mixing ratio perturbations $[\frac{\partial (P-L)}{\partial r}]$, respectively. The latter term is often expressed in terms of the photochemical relaxation time for ozone, $\tau_{O_3} = -[\frac{\partial (P-L)}{\partial r}]^{-1}$.

Figure 6 plots $(P-L)_o$ and τ_{O_3} calculated with the NRL CHEM2D model for mid-January conditions. In general, CHEM2D $(P-L)_o$ values are in good agreement with those of Fleming et al. (2001) that are used in both the NASA GEOS4 data assimilation

ACPD
4, 4227–4284, 2004

system and in the NCEP GFS model. Because the temperature and column ozone effects are generally smaller in comparison with the first two terms on the right hand side of Eq. (1), ozone simulations over 5 day periods using the CHEM2D scheme that neglects these terms should not be a seriously affected. Cariolle and Deque (1986) have shown that inclusion of the temperature and column ozone terms is important for longer simulations over seasonal and interannual time scales.

3. Data description

As a first test of the new NOGAPS-ALPHA model performance, we compare simulations of stratospheric ozone and temperature for select periods during the SOLVE2 campaign with observations from a variety of sources. These sources include operational ECMWF meteorological analyses, satellite-based measurements of the total ozone column abundance and ozone profiles, and data records from instruments aboard the NASA DC-8 aircraft. A short description of each data source follows.

3.1. Meteorological analyses

During the SOLVE2 period, operational NOGAPS analyses from the MVOI system (Goerss and Phoebus, 1992) were made available at 0, 6, 12, and 18 Z. These gridded ($1^{\circ} \times 1^{\circ}$ latitude/longitude) fields include horizontal winds, temperature, geopotential height, vorticity, and divergence on a fixed set of pressure levels extending up to 10 hPa. In addition, archived high-resolution (T511L60) operational analyses from the ECMWF Integrated Forecast System (IFS) provided twice daily (0 Z and 12 Z) winds, temperature, geopotential height, vorticity, divergence, and ozone mass mixing ratio (ECMWF, 1995). The ECMWF fields are stored on native model levels (see, e.g. Dethof, 2003) using a reduced (N256) Gaussian grid. For both the 14 January and 21 January case studies in the present work, operational T239L30 NOGAPS and T511L60 ECMWF meteorological analyses are used to asses the performance of the

ACPD
4, 4227–4284, 2004

new NOGAPS-ALPHA model.

NOGAPS-ALPHA ozone simulations use 3-D stratospheric ozone analyses output from the operational NASA GEOS4 data assimilation system to initialize both the active and passive ozone fields (Stajner et al., 2001, 2004). Daily global GEOS4 ozone analyses at 0 Z were made available throughout the SOLVE2 winter at fixed pressure levels from 1000 hPa to 0.2 hPa with a $2^{\circ} \times 2.5^{\circ}$ latitude/longitude resolution. The GEOS4 system assimilates stratospheric ozone profiles and total ozone column measurements from the NOAA-16 SBUV/2 instrument. Ozone photochemical production and loss rates are specified as functions of latitude, pressure, and month (Fleming et al., 2001), with adjustments to the upper stratospheric values as in Stajner et al. (2004).

The operational ECMWF ozone assimilation (Dethof, 2003) product is based on NOAA-16 SBUV/2 profile and ERS-2 GOME total ozone measurements and uses the linearized ozone photochemistry scheme of Cariolle and Deque (1986). Results from a series of 5-day NOGAPS-ALPHA ozone simulations in Sect. 4 show that these differences between the GEOS4 and ECMWF ozone assimilation systems at high latitudes can lead to large differences in the ozone forecast skill.

3.2. Satellite ozone measurements

The present study compares NOGAPS-ALPHA prognostic ozone simulations with measurements of the integrated column ozone abundance the Total Ozone Mapping Spectrometer (TOMS) aboard the NASA Earth Probe satellite (McPeters et al., 1998). Since the largest contribution to the total ozone column originates in the lower stratosphere, where the ozone photochemistry is slow compared to transport, this quantity provides a good test of the model's spectral transport.

Observations of the vertical distribution of ozone comes from the NASA Stratospheric Aerosol and Gas Experiment (SAGE) III instrument aboard the METEOR-3M satellite (Thomason and Taha, 2003), and from the NRL Polar Ozone and Aerosol Monitoring (POAM) III instrument aboard the CNES SPOT-4 satellite (Bevilacqua et

al., 2002). Both satellites operate in sun-synchronous orbits that offer excellent coverage of polar latitudes during winter. For the 11–22 January 2003 period, SAGE III provides 13 to 14 profiles each day over latitudes ranging from 67° N–69° N. The present study uses the Version 3.04 "least squares" SAGE III retrievals between 200–1 hPa. For the same time period, POAM III provides 14 to 15 stratospheric profiles (Version 3) each day from 250–0.1 hPa over the 64° N–65° N latitude range. The combined random and systematic errors in the stratospheric ozone profiles are <5% for both instruments. Both SAGE III and POAM III retrievals provide profiles of ozone molecular concentration that are converted to volume mixing ratio using temperature and pressure analyses. SAGE III retrievals use temperature and pressure information from the National Centers for Atmospheric Prediction (NCEP) up to 1 hPa. POAM III retrievals use temperature and pressure information provided by the United Kingdom Meteorological Office (UKMO). Section 4 compares NOGAPS-ALPHA ozone hindcasts for 11–16 January 2003 (Case 1) with EP-TOMS, SAGE III, and POAM III observations as well as ECMWF operational ozone analyses and forecasts.

3.3. DC-8 measurements

Of the 14 different experiments on the NASA DC-8 aircraft payload for SOLVE2, two are particularly well-suited for comparison with NOGAPS-ALPHA simulations. The first experiment is the NASA Langley Differential Absorption Lidar (DIAL). DIAL measures backscattered radiation near wavelengths of 301 nm and 311 nm, providing in-flight ozone profiles with a vertical resolution of 750 m over the altitude region from ~1 km above the aircraft up to 22–26 km under ideal conditions (Grant et al., 2003). The second experiment is the NASA Goddard Airborne Raman Ozone Temperature and Aerosol Lidar (AROTAL). AROTAL uses a combination of Rayleigh and Raman backscattered radiation at 355 nm to retrieve temperature profiles up to 60 km with a vertical resolution of 0.5–1.5 km (Burris et al., 2002). This instrument also utilizes a differential absorption technique to obtain ozone profiles up to ~30 km, even in the presence of aerosols and clouds. Section 5 presents a combination of both DIAL

ACPD
4, 4227–4284, 2004

and AROTAL ozone profiles as a means of validating high resolution T239 NOGAPS-ALPHA prognostic ozone simulations along the DC-8 flight track during the 21 January 2003 stratospheric warming case (i.e. Case 2).

4. Case 1: 11–16 January 2003

4.1. Description

As Fig. 1 shows, 30 hPa temperatures over the polar region were cold enough to promote PSC formation during the early winter of 2002–2003. The DC-8 flight on 14 January 2003 was the last to take place before the stratospheric warming event in mid-January. During the 14 January flight, instruments aboard the DC-8 detected a small region of PSC's over the southern tip of Scandinavia.

Figure 7a plots NOGAPS analyses of 30 hPa temperatures and geopotential heights on 14 January 2003. The region where PSC's were detected lies within a larger synoptic-scale area of cold temperatures. Figure 7b plots the corresponding temperatures and heights at 300 hPa, showing a pronounced anti-cyclonic feature over Western Europe. This type of feature produces a combination of upward vertical motion and quasi-isentropic horizontal transport in the lowermost stratosphere, leading to a divergence of ozone-rich air out of the column (see, e.g. Rood et al., 1992; Orsolini et al., 1995). These localized, reversible occurrences of low total ozone, often referred to as extreme ozone minima or ozone "mini-holes", are common occurrences with the passage of an intense upper tropospheric anticyclone (Newman et al., 1988; McCormack and Hood, 1997; James, 1998). In certain cases, the resulting adiabatic cooling in the lower stratosphere can be sufficiently strong to produce temperatures below 195 K, which is a typical threshold temperature for the formation of nitric acid trihydrate (NAT) particles that constitute Type I PSC's (Teitelbaum et al., 2001; WMO, 2003).

Figure 8 plots total ozone column measurements from the NASA EPTOMS instrument on 14 January 2003. The heavy red contour highlights the total ozone mini-

ACPD
4, 4227–4284, 2004

mum near 10° W–30° E longitude where total ozone values fall below 235 Dobson units (DU). This region coincides with the minimum in 30 hPa temperatures and maximum in 300 hPa geopotential heights shown in Fig. 7. Conditions on 14 January 2003 provide a good first test of the ability of NOGAPS-ALPHA to simulate this interaction between tropospheric and stratospheric dynamics and its impact on the ozone distribution.

To determine the sensitivity of the model ozone simulations to the linearized photochemistry parameterization, we conducted a series of low-resolution T79 (~1.5° latitude/longitude spacing) simulations using three different sets of linearized photochemistry coefficients. These include an updated version of the CD86 scheme currently used in the ECMWF model (H. Teyssedre, personal communication), the LINOZ scheme, and the NRL CHEM2D scheme (see Sect. 2.6 for details). Our goal is to determine which scheme most closely reproduces the observed 3D ozone distribution poleward of 20° N latitude on 14 January 2003.

4.2. Comparison with ozone analyses

For each simulation, both active and passive ozone fields were initialized using ozone mixing ratio analyses from the NASA GEOS4 system (Stajner et al., 2001, 2004). Figure 9a plots the initial NOGAPS-ALPHA active/passive ozone mixing ratios as a function of pressure and longitude at 64.9° N latitude on 11 January 2003. At this latitude, the initial NOGAPS-ALPHA ozone distribution differs substantially from the ECMWF ozone analyses for the same day and same location plotted in Fig. 9b. Specifically, the ECMWF ozone mixing ratios exceed the NASA GEOS4 mixing ratios by more than 2 ppmv between 30° W–30° E longitude. Figure 9c shows a series of ozone mixing ratio profiles from the POAM III instrument on 11 January 2003. The POAM III measurements confirm the presence of low ozone mixing ratios between 30° W–30° E longitude not captured in the ECMWF analyses.

This discrepancy between the GEOS4 and ECMWF ozone analyses over the North Atlantic sector is common throughout the SOLVE2 period poleward of ~60° N latitude; at lower latitudes, however, both the ECMWF and GEOS4 ozone products are in good

ACPD
4, 4227–4284, 2004

agreement. Although the exact cause of this discrepancy is not known, it should be noted that the GEOS4 system (Stajner et al., 2001) assimilates SBUV/2 total ozone measurements whereas the ECMWF system (Dethof, 2003) assimilates total ozone from the GOME instrument, which has a lower spatial sampling rate. It may be that such differences in the details of the total ozone assimilation may contribute to differences in the analyzed ozone product even in polar regions where the measurements themselves are not directly applied.

4.3. NOGAPS-ALPHA O_3 forecasts 11–17 January 2003

Figure 10 plots NOGAPS-ALPHA profiles of prognostic ozone for a 5-day simulation initialized on 11 January 2003 over Kiruna, Sweden (68° N, 20° E). This location was chosen for its proximity to both the lowest total ozone values on 14 January and the measurement latitudes of the SAGE III and POAM III instruments (see Fig. 8). Each plot compares the passive ozone (dashed black curve) with active ozone computed using the CD86 coefficients (blue curve), the LINOZ coefficients (red curve), and the CHEM2D coefficients (green curve). Also included in Fig. 10 are the ECMWF ozone forecasts (solid black curve) and co-located ozone profiles from the SAGE III instrument (points) for each day. As Fig. 10 shows, the differences between the GEOS4 and ECMWF ozone initializations at this location on 11 January 2003 explain why the ECMWF ozone forecasts over the 5-day period disagree with the NOGAPS-ALPHA simulations and with the independent SAGE III measurements between 50–1 hPa. Interestingly, the ECMWF ozone profiles show better agreement with the SAGE III profiles then corresponding NOGAPS-ALPHA ozone profiles between 50–100 hPa.

A comparison of the active ozone simulations (blue, red, and green curves in Fig. 10) shows all three photochemistry schemes exhibit little difference with the passive ozone profile below ~10 hPa. In this altitude region, there is generally good agreement among the three different active ozone schemes, passive ozone, and observed ozone profiles from both the SAGE III and POAM III instruments. This is to be expected since ozone photochemistry is slow compared to transport below ~10 hPa.

Above ∼10 hPa, where photochemistry dominates over transport, differences emerge between the active and passive ozone values, and between the individual active ozone simulations as well. The differences between the CD86 and CHEM2D results after 5 days are very small, and they are both in good agreement with the SAGE III measurements shown in Fig. 10. The similarity between the CHEM2D and CD86 profiles in Fig. 10 demonstrates that neglecting the temperature and column terms in Eq. (1) have a minor impact on the model ozone over 5 days. In contrast, the LINOZ scheme produces excessive ozone loss that is in disagreement with the available SAGE III profiles, POAM III profiles (not shown), and with the NOGAPS-ALPHA simulations using CHEM2D and CD86 photochemistry schemes.

The low upper stratospheric ozone mixing ratios in the NOGAPS-ALPHA simulation using the LINOZ scheme (red curve in Fig. 10) appears to be a consequence of unrealistically large negative values in the LINOZ scheme's $(P-L)_o$ term. As Fig. 6 illustrates, the net ozone mixing ratio tendency $(P-L)_o$ at high northern latitudes during January is typically small, less than -1 ppmv month^{-1} above 10 hPa and poleward of 60° N. In comparison to both the CD86 and CHEM2D coefficients, the LINOZ $(P-L)_o$ term is 5–10 times more negative at all latitudes above ∼10 hPa for all months. The underlying cause for the excessive LINOZ ozone loss above 10 hPa may be related to an overestimation of the background ozone mixing ratios in the model (McLinden et al., personal communication). Overall, the results from the initial NOGAPS-ALPHA prognostic ozone simulations indicate that the LINOZ photochemistry parameterization may not be appropriate for upper stratospheric applications.

Figure 11 plots NOGAPS-ALPHA model ozone mixing ratio profiles at 65° N and 135° E from the same 5-day simulation beginning 11 January 2003. Here we compare results from the three different ozone photochemistry schemes, passive ozone, the ECMWF ozone forecasts, and POAM III ozone profiles. Unlike the previous case, the initial NOGAPS-ALPHA ozone mixing ratio profiles and ECMWF operational ozone analyses on 11 January over this location are in good agreement. Total ozone values on 14 January (forecast hour 96) were greater than 475 DU over this location, and the

ACPD
4, 4227–4284, 2004

flow around at mid-stratospheric levels (see Fig. 7) brought air from lower sunlit latitudes poleward. Thus the ozone photochemistry parameterization should have more of an impact on the ozone profiles at this location than for the ozone profiles over Kiruna (see Fig. 10) where mid-stratospheric air was largely confined within polar night.

As Fig. 11 shows, the NOGAPS-ALPHA ozone simulations using the LINOZ scheme again produce excessive ozone loss above 10 hPa over the course of 2–3 days. However, significant differences can also be seen between the results from the CD86 and CHEM2D schemes. By hour 96, both the CD86 results and the ECMWF operational ozone forecasts (which use the CD86 scheme) produce ozone mixing ratios between 10 hPa and 50 hPa that are up to 2 ppmv less than values from either the CHEM2D or LINOZ schemes or the model passive ozone. Above 10 hPa, the LINOZ scheme again produces excessive ozone loss as compared to the POAM profiles. Both CHEM2D and passive ozone profiles agree well with POAM observations, especially at hours 96 and 120.

For the ozone simulations over 65° N and 135° E shown in Fig. 11, the initial ozone profiles agree quite well. The main differences between the NOGAPS-ALPHA simulations using the CD86 and CHEM2D parameterizations are in the details of the photochemical parameterization (see Eq. 1). Specifically, these differences are in the values of the photochemical relaxation time τ_{O_3} in the midlatitude lower stratosphere. At this location, the model ozone mixing ratios exceed 2-D climatological values (r_o) and so the ozone tendency is negative (see Eq. 1). Typically, values of τ_{O_3} exceed 100 days in the midlatitude stratosphere near 25 km (Brasseur and Solomon, 1986). In the CD86 scheme (see, e.g. Cariolle and Deque, 1986, their Fig. 3), these values are 30–50 days. The shorter relaxation times of the CD86 scheme causes lower stratospheric ozone mixing ratios in the midlatitudes to relax back to climatology 2–3 times faster than in either the CHEM2D or LINOZ schemes. It is interesting to note that both the ECMWF and NOGAPS-ALPHA model ozone exhibit the same tendency toward lower ozone when the latter model employs the CD86 scheme.

Next, high resolution T239 NOGAPS-ALPHA simulations of both active (using the

CHEM2D scheme) and passive ozone were conducted for the same 5-day period starting on 11 January 2003. Figure 12a plots the forecast total ozone distributions at hour 96, valid at 0 Z 14 January 2003, computed from NOGAPS-ALPHA prognostic ozone using the CHEM2D photochemistry scheme and initialized with the NASA GEOS4 operational ozone analyses. This NOGAPS-ALPHA total ozone field exhibits very good qualitative and quantitative agreement with the EPTOMS total ozone distribution for 14 January (Fig. 8). Specifically, the NOGAPS-ALPHA simulations in Fig. 12a reproduce the regions of low total ozone (<235 DU) over the North Atlantic sector, high total ozone (>475 DU) over Siberia (65° N, 135° E), and the "arm" of 370–420 DU values extending eastward from the Mediterranean all present in the EP-TOMS observations in 14 January.

Figure 12b plots the corresponding 96-h operational ECMWF forecast total ozone distribution initialized on 11 January 2003 and valid for 0 Z 14 January 2003. In comparison with the NOGAPS-ALPHA and EPTOMS total ozone fields, the ECMWF total ozone forecast for this time exhibits much smoother zonal structure in the total ozone at middle and high latitudes. Furthermore, the ECMWF total ozone values for this date fails to fully capture the observed area of total ozone values below 235 DU over the North Atlantic sector.

To understand the origins of the differences between the NOGAPS-ALPHA and ECMWF total ozone forecasts (Figs. 12a and b, respectively), we performed an additional NOGAPS-ALPHA simulation using the CD86 photochemistry scheme and initialized with the ECMWF operational ozone analyses. The largest contribution to the total ozone column abundance comes from the lower stratosphere (i.e. 10–20 km altitude), where transport effects tend to dominate over photochemistry. By using ozone photochemistry and initial conditions similar to the operational ECMWF model, we can be reasonably sure that the only major differences between this NOGAPS-ALPHA experiment and the ECMWF results should be due to differences in model lower stratospheric transport. Figure 12c plots the resulting NOGAPS-ALPHA 96-h total ozone forecast using the CD86 scheme and ECMWF ozone initialization. This result bears a

ACPD
4, 4227–4284, 2004

very close resemblance to the operational 96-h ECMWF total ozone forecast shown in Fig. 12b, indicating that spectral transport in the T239 NOGAPS-ALPHA model compares quite well with the operational ECMWF model in the lower stratosphere for this case.

An additional low-resolution T79 NOGAPS-ALPHA total ozone simulation using the CD86 photochemistry scheme with the NASA GEOS4 ozone initialization (not shown) partially reproduces the observed ozone minima over the North Atlantic. However, this same experiment also exhibits zonal structure in total ozone that is much smoother than both 96-h NOGAPS-ALPHA total ozone using the CHEM2D scheme and 14 January EP-TOMS observations. This result indicates that the differences between the CD86 and CHEM2D photochemistry schemes can indeed impact model ozone in the lower stratosphere over the course of several days. Specifically, the CD86 scheme tends to relax lower stratosphere ozone back to a zonal mean basic state more quickly than either the CHEM2D scheme.

Based on these results, we find that the major differences between operational ECMWF and NOGAPS-ALPHA ozone simulations for the 11–17 January case are due to (1) ECMWF ozone analyses not capturing the observed ozone minimum over the North Atlantic sector in the model initial conditions for 11 January 2003 (see Fig. 9); and (2) shorter stratospheric ozone photochemical relaxation times τ_{O_3} in the CD86 scheme as compared to either the CHEM2D or LINOZ schemes.

5. Case 2: 17–22 January 2003

5.1. Description

Case 2 corresponds to the early period of the stratospheric warming that characterized the SOLVE2 winter (Fig. 1). As shown in Fig. 13, the polar vortex had split into two lobes by 21 January. This disturbed stratospheric meteorology during 17–21 January presents an excellent test for the NOGAPS-ALPHA GCM generally, and its internal

ACPD
4, 4227–4284, 2004

spectral chemical advection scheme specifically. An earlier study of prognostic skill in the lower stratosphere by Lahoz (1999) using various high-altitude versions of the United Kingdom Meteorological Office (UKMO) Unified Model focused on hindcasting during February 1994. This period yielded a minor wave-2 warming with a split vortex structure very similar morphologically to that seen in Fig. 13 (see, e.g. Lahoz's Fig. 7c).

Lahoz (1999) noted that the UKMO models' NWP skill tended to be poorest during this period of rapidly evolving mean flow, and cited these cases as requiring careful scrutiny when operational forecasts were used to plan aircraft flights for Arctic science missions.

Thus, in light of this previous work, the 17–21 January period presents a highly relevant case for studying model performance within the context of airborne SOLVE2 science flights. Furthermore, the rapid dynamical evolution of this case also provides a fairly rigorous test case for our new spectral advection formulation for transporting ozone. To assess the advection code's performance using ozone as our diagnostic model variable, we will study prognostic ozone in the lower stratosphere only, where photochemical lifetimes at all latitudes are long compared to forecasting timescales.

5.2. Lidar ozone profiles from SOLVE2 DC-8 flight

To validate NOGAPS-ALPHA's prognostic ozone during Case 2, we utilize DC-8 data acquired during a science flight on 21 January 2003 (see Fig. 14). For comparison, we have chosen two flight segments for detailed analysis. The first flight segment, denoted FS-1, is shown in light-orange in Fig. 14. From Fig. 13, we see that first part of FS-1 heads away from the split polar vortices as the aircraft flies south of Iceland from Kiruna. The second part of FS-1 then heads back into the split polar vortices as the DC-8 proceeds north toward Greenland. The second flight segment (FS-2) involves an approximately linear transect from southern Greenland to Svalbard, flying across the split vortex lobe structures shown in Fig. 13. FS-2 potentially profiles mid-latitude low-PV air from a filament separating the two lobes at the approximate midpoint of this flight segment.

ACPD
4, 4227–4284, 2004

Figures 15 and 16 plot ozone mixing ratios acquired along FS-1 and FS-2, respectively, from the DIAL and AROTAL lidar systems on board the DC-8. Both lidar systems reproduce the same major features. For FS-1, the lidar data in Fig. 15 show ozone mixing ratios in the lower stratosphere decreasing as the DC-8 heads southwest to Iceland, then increasing substantially through the stratosphere during part of its northward trek toward the coast of Greenland. For FS-2, mixing ratios are generally smaller, with upper-level mixing ratios decreasing along the flight transect. Near the midpoint of FS-2, both lidars show a sloping upward bulge of low ozone air at ~15 km and a narrow increase in ozone mixing ratio at ~19:20 Z at heights ~15–20 km and, in AROTAL, again at ~30 km. This seems to be a possible ozone signature of the filament of low-PV air separating the split vortex lobes, noted in Fig. 13.

5.3. Comparison with ozone analyses

We begin by comparing the ECMWF and GEOS4 ozone analyses along the DC-8 flight track to determine if either system captures any of the features seen in the DC-8 lidar data. Accordingly, Fig. 17 plots ozone mixing ratios for 21 January 2003 from the GEOS4 analysis (at 12 Z) and the operational ECMWF analysis (at 18 Z), these two times roughly spanning the 13–16 Z period of FS-1. Note the much coarser spatial resolution of the GEOS4 ozone analysis that provides initial conditions for prognostic ozone in NOGAPS-ALPHA. Both analyses capture the downward sloping ozone isopleths at ~20–30 km. The ECMWF analysis also captures the reduction in ozone at ~20 km from ~13:30–14:30 Z and the sudden increase at ~14:30 Z.

Figure 18 plots ozone analyses along FS-2, using 18 Z fields for both analyses in this case. Both analyses capture large ozone mixing ratios at upper levels at the start of the flight segment, and progressive reductions in these mixing ratios along the flight track. Near the midpoint of the flight, the higher-resolution ECMWF ozone analysis also shows what appears to be an ozone signature of the PV filament separating the two vortex lobes. At ~15 km and ~30–35 km, the structure is very similar to that seen in the lidar data in Fig. 16. At ~20 km, however, the lidar data show an ozone enhancement

ACPD
4, 4227–4284, 2004

at 19:00–19:30 Z, whereas the analyzed ECMWF ozone shows a slight depletion.

5.4. NOGAPS-ALPHA ozone forecast fields

Since NOGAPS-ALPHA is initialized with the coarse resolution GEOS4 ozone product shown in Figs. 17a and 18a, it is not clear whether the higher-resolution (T239L54) NOGAPS-ALPHA model dynamics can reproduce observed finer-scale features in the DC-8 lidar ozone profiles. This section presents NOGAPS-ALPHA prognostic ozone fields along the selected DC-8 flight tracks on 21 January.

Figure 19 plots NOGAPS-ALPHA prognostic ozone fields along FS-2 for the 114-h forecast initialized on 17 January at 0 Z (valid on 21 January 2003 at 18 Z, the approximate time of FS-2). The two panels plot the same data, first as a function of pressure altitude, then as a function of geopotential altitude. Geopotential heights are more directly comparable to the geometric altitudes at which the lidar ozone data are registered in Fig. 16. Figure 19 shows that lower stratospheric pressure altitudes are typically ∼2–4 km higher than the corresponding geopotential height altitudes. This vertical offset between lidar geometric altitudes and model pressure altitudes should be borne in mind during the subsequent along-track ozone comparisons.

Despite initialization with the lower-resolution GEOS4 ozone analysis, the NOGAPS-ALPHA 114-h hindcast of ozone mixing ratios along FS-2 in Fig. 19b shows interesting similarities to the DC-8 lidar data in Fig. 16. In particular, the forecast reproduces the sloping low-ozone bulge at ∼14 km at ∼18:30–19:00 Z, and also produces an isolated ozone enhancement in the lower stratosphere, starting at ∼19–20 km and extending upwards, similar to what is seen in the lidar data in Fig. 16. These features arise in the NOGAPS-ALPHA forecast when the vortex splits and a thin filament of mid-latitude air is drawn polewards, separating the two vortex lobes. However, the width of this NOGAPS-ALPHA ozone enhancement is broader in this 114-h forecast than the actual ozone filament width seen in the lidar profiles.

Figure 20 plots the corresponding archived T511L60 ECMWF 114-h ozone forecast for 21 January 2003 at 18 Z. This forecast yields an ozone filament, but its location

ACPD
4, 4227–4284, 2004

along the flight track is incorrect by 30–60 min; the sloping low-ozone enhancement occurs at ~19:30–20:00 Z and the stratospheric ozone anomalies due to the filament occur towards the end of the flight segment at ~20:40 Z. The location of this ozone anomaly along the flight track significantly improves with the +90-h ECMWF forecast (not shown).

One major difference between the ECMWF and NOGAPS-ALPHA ozone simulations for this date is that the ECMWF ozone forecasts improve with each forecast update more noticeably than do the NOGAPS-ALPHA ozone forecasts. Figure 21 plots 42-h forecasts along FS-2 from both the archived T511L60 ECMWF forecasts and NOGAPS-ALPHA hindcasts initialized with GEOS4 analysis ozone on 20 February at 0 Z. The filament features are much less well resolved in the NOGAPS-ALPHA forecast than for ECMWF.

One possible explanation for this difference may be that the ECMWF system employs very high horizontal resolution whereas the present NOGAPS-ALPHA simulations use the NASA GEOS4 ozone analyses at a much coarser horizontal resolution for initialization in NOGAPS-ALPHA (Fig. 18). Longer forecasts are less influenced by model initial conditions and more influenced by model physics. For shorter forecasts, the opposite is true. It is possible that the lower horizontal resolution of the NOGAPS-ALPHA ozone initialization imposes a greater limitation on ozone forecasts as these forecasts are initialized progressively closer to the actual flight time and thus are run for a shorter time.

To explore this possibilty, we next profile an N_2O-like chemical tracer that, along with active and passive ozone, is a standard NOGAPS-ALPHA prognostic chemical constituent. These fields of "pseudo-N_2O" are initialized from a two-dimensional nitrous oxide climatology and are photochemically updated using parameterized N_2O loss based on output from the NRL CHEM2D model (McCormack and Siskind, 2002), similar to the approach outlined in Randel et al. (1994) (see also Eckermann et al., 2004b). Given this two-dimensional climatological initialization, it must be stressed that this is not a true N_2O forecast. Nonetheless, the sharp initial meridional and vertical

gradients in this initial two-dimensional pseudo-N_2O field make it an excellent diagnostic in NOGAPS-ALPHA for the 17–21 January case.

Figure 22 plots the 42-h hindcast of these psuedo-N_2O mixing ratios along flight segment 2. The similarity between the mid-flight isopleth filament structure seen here and that seen in the ECMWF 42-h ozone forecast in Fig. 21b suggests that our prognostic meteorological transport is similar to ECMWF's in this case. This similarity supports the assertion that the coarse resolution in the NOGAPS-ALPHA ozone initialization (based on the GEOS4 analyses) may explain similar coarse resolution in the 42-h NOGAPS-ALPHA ozone forecast in Fig. 21a.

Figure 23 plots a synoptic map of the NOGAPS-ALPHA 42-h ozone forecast at 26.7 hPa on 21 January 2003 at 18 Z. The DC-8 flight track for this date is included for reference. This map shows a tongue of high ozone air near southern Greenland that has wrapped around the western vortex lobe and intercepts FS-1 near the end of this flight segment. This accounts for the sudden increase in stratospheric ozone mixing ratios observed in the FS-1 lidar data at 15 Z (Fig. 15) near the end of this flight segment. Figure 23 also indicates both high and low ozone filaments intersecting the midpoint of FS-2 between the two separated vortex lobes containing low ozone mixing ratios forecast in this run.

6. Summary and conclusions

We have tested the new prognostic ozone component of the NOGAPS-ALPHA middle atmosphere forecast model for two distinct cases during the 2003 SOLVE II campaign: (1) 11–16 January 2003, when the polar vortex was relatively cold and stable; and (2) 17–22 January 2003, when a rapidly developing stratospheric warming split the vortex into two separate lobes. Initial comparisons of NOGAPS-ALPHA 5-day stratospheric ozone hindcasts with a combination of satellite and aircraft measurements of polar ozone indicate that the performance of the new prognostic ozone for these two cases is comparable to current operational ECMWF ozone forecasts. Specific results for the

ACPD
4, 4227–4284, 2004

individual cases are summarized below.

For the case of 11–16 January 2003, an intercomparison of three different linearized ozone photochemistry schemes found that all three schemes generated forecast ozone profiles in good agreement with the SAGE III and POAM III solar occultation measurements at high latitudes at and below 10 hPa. Above 10 hPa, NOGAPS-ALPHA ozone simulations using the LINOZ scheme of McLinden et al. (2000) generated excessive ozone losses over the course of the 5-day forecast in disagreement with observations. These losses are evident at all latitudes above 10 hPa, and suggest that the LINOZ scheme may not be suitable for upper stratosphere applications. At middle latitudes receiving more sunlight, significant differences were found between NOGAPS-ALPHA ozone forecasts using the NRL-CHEM2D and CD86 (i.e. Cariolle and Deque, 1986) ozone photochemistry parameterizations. Specifically, the CD86 scheme produced a smoother zonal structure in lower stratospheric ozone, most likely due to the shorter ozone photochemical relaxation times inherent in the CD86 formulation. A comparison of the NOGAPS-ALPHA prognostic ozone simulations with operational ECMWF ozone forecasts found significant differences due to different model ozone initial conditions. NOGAPS-ALPHA ozone forecasts initialized with the NASA GEOS4 ozone analyses produced much better agreement with satellite measurements at high latitudes than did the operational ECMWF ozone forecasts, particularly in the longitude sector between 10° W–30° E.

For the case of 17–22 January 2003, NOGAPS-ALPHA 114-h forecasts of stratospheric ozone along the DC-8 flight track of 21 January produced agreement with DC-8 DIAL and AROTAL ozone profiles which was as good or slightly better than corresponding ECMWF ozone forecasts. Updated (e.g. 42-h) ECMWF ozone forecasts for 21 January rapidly improved their simulation of the split vortex and subsequent fine structure in stratospheric ozone mixing ratios; NOGAPS-ALPHA ozone forecasts, on the other hand, did not show such improvement. This is most likely due to the coarser resolution of the ozone analyses used to initialize NOGAPS-ALPHA prognostic ozone, which exerts a greater influence on short-term forecasts (i.e. 42-h) than on longer-term

ACPD
4, 4227–4284, 2004

(i.e. 114-h) forecasts.

Overall, the good agreement between NOGAPS-ALPHA prognostic ozone and both satellite and DC-8 aircraft measurements during the SOLVE2 campaign demonstrate that the model's spectral transport and parameterized photochemistry are capable of providing reliable short-range ozone forecasts. More detailed, quantitative assessments of NOGAPS-ALPHA forecast skill in the troposphere and stratosphere are currently underway. Future work will include development of the temperature and column ozone terms in the NRL-CHEM2D linearized ozone photochemistry scheme and on improvements in the ozone initialization. The ultimate goal of this work is a fully operational prognostic ozone scheme for the assimilation of satellite radiance measurements.

Acknowledgements. This research was supported in part by the Office of Naval Research 6.1 and 6.2 programs and by the NASA Office of Earth Science. Thanks to I. Stajner at the NASA Global Modeling and Assimilation Office for providing access and helpful discussions regarding the GEOS4 ozone analyses, and to D. Siskind at NRL for guidance with the CHEM2D model.

References

Alexander, M. J. and Dunkerton, T. J.: A spectral parameterization of mean-flow forcing due to breaking gravity waves, J. Atmos. Sci., 56, 4167–4182, 1999.

Baker, N. L.: Quality control for the Navy operational atmospheric database, Wea. Forecasting, 7, 250–261, 1992. 4229

Baldwin, M. P. and Dunkerton, T. J.: Stratospheric harbingers of anomalous weather regimes, Science, 294, 581–584, 2001.

Bevilacqua, R. M., Fromm, M. D., Alfred, J. M., Hornstein, J. S., Nedoluha, G. E., Hoppel, K. W., Lumpe, J. D., Randall, C. E., and Shettle, E. P.: Observations and analysis of PSCs detected by POAM III during the 1999/2000 northern hemisphere winter, J. Geophys. Res., 107(20), 8281, doi:10.1029/2001JD000477, 2002. 4240

Boville, B. A.: Wave-mean flow interactions in a general circulation model of the troposphere and stratosphere, J. Atmos. Sci., 43, 1711–1725, 1986. 4235

Braesicke, P., Jrrar, A., Hadjinicolaou, P., and Pyle, J.: Variability of total ozone due to the NAO as represented in two different model systems, Met. Z., 12, 203–208, 2003. 4231
Brasseur, G. and Solomon, S.: Middle Atmospheric Chemistry, Aeronomy of the Middle Atmosphere, D. Reidel, Norwell, MA, USA, 2nd ed., 452, 1986. 4246
Burris, J., McGee, T., Hoegy, W., et al.: Validation of temperature measurements from the airborne Raman ozone temperature and aerosol lidar during SOLVE, J. Geophys. Res., 107(D20), doi:10.1029/2001JD001028, 2002. 4241
Butchart, N. and Austin, J.: Middle atmosphere climatologies from the troposphere-stratosphere configuration of the UKMO's unified model, J. Atmos. Sci., 55, 2782, 1998. 4235
Cariolle, D. and Deque, M.: Southern hemisphere medium-scale waves and total ozone disturbances in a spectral general circulation model, J. Geophys. Res., 91, 10 825–10 846, 1986. 4238, 4239, 4240, 4246, 4254
Chou, M.-D. and Suarez, M. J.: A solar radiation parameterization for atmospheric studies, NASA Tech. Mem. 10460, 15, Technical Report Series on Global Modeling and Data Assimilation, edited by Suarez, M. J., 52, 2002. 4234
Chou, M.-D., Suarez, M. J., Liang, X. Z., and Yan, M.-H.: A thermal infrared radiation parameterization for atmospheric studies, NASA Tech. Mem. 104606, 19, Technical Report Series on Global Modeling and Data Assimilation, edited by Suarez, M. J., 65, 2001. 4234
Chun, H.-Y. and Baik, J. J.: An updated parameterization of convectively forced gravity wave drag for use in large-scale models, J. Atmos. Sci., 59, 1006–1017, 2002. 4235
Daley, R. and Barker, E.: NAVDAS: formulation and diagnostics, Mon. Wea. Rev., 129, 869–883, 2001. 4229, 4230
Derber, J. C. and Wu, W.-S.: The use of TOVS cloud-cleared radiances in the NCEP SSI analysis system, Mon. Wea. Rev., 126, 2287–2299, 1998. 4230
Dethof, A.: Aspects of Modelling and Assimilation for the Stratosphere at ECMWF, SPARC Newsletter 21, http://www.aero.jussieu.fr/~sparc/News21/21_Dethof.html, 2003. 4231, 4239, 4240, 4244
Dethof, A. and Holm, E.: Ozone in ERA-40: 1991–1996, European Centre for Medium-Range Forecasts Technical Memorandum No. 377, Reading, England, 37, 2002. 4238
Eckermann, S. D., Ma, J., and Broutman, D.: The NRL Mountain Wave Forecast Model (MWFM), Preprint Vol., Symposium on the 50th Anniversary of Operational Numerical Weather Prediction, American Meteorological Society, University of Maryland, College Park,

MD, 14–17 June, 20, in press, 2004a. 4229
Eckermann, S. D., McCormack, J. P., Coy, L., Allen, D., Hogan, T., and Kim, Y.-J.: NOGAPS-ALPHA: A prototype high-altitude global NWP model, Preprint Vol., Symposium on the 50th Anniversary of Operational Numerical Weather Prediction, American Meteorological Society, University of Maryland, College Park, MD, 14–17 June, 23, in press, 2004b. 4229, 4252
ECMWF: The Description of the ECMWF/WCRP Level III-A Global Atmospheric Data Archive, ECMWF Operations Department, Shinfield Park, Reading, Berkshire, RG3, 9AX, England, 1995. 4239
Emanuel, K. A. and Zivkovic-Rothman, M.: Development and evaluation of a convection scheme for use in climate models, J. Atmos. Sci., 56, 1766–1782, 1999. 4233
Errico, R. M., Barker, E. H., and Gelaro, R.: A determination of balanced normal modes for two models, Mon. Wea. Rev., 116, 2717–2724, 1988. 4229
Fairlie, T. D. A., Turner, R. E., and Siskind, D. E.: Transport characteristics of a finite difference dynamics model combined with a spectral transport model of the middle atmosphere, Mon. Wea. Rev., 122, 2363–2375, 1994. 4237
Fleming, E. L., Chandra, S., Barnett, J. J., and Corney, M.: Zonal mean temperature, pressure, zonal wind, and geopotential height as functions of latitude, COSPAR International Reference Atmosphere: 1986, Part II: Middle Atmosphere Models, Adv. Space Res., 10(12), 11–59, 1990. 4236
Fleming, E., Jackman, C., Considine, D., and Stolarski, R.: Sensitivity of tracers and a stratospheric aircraft perturbation to two-dimensional model transport variations, J. Geophys. Res., 106(D13), 14 245–14 264, doi:10.1029/2000JD900732, 2001. 4238, 4240
Fortuin, J. P. F. and Kelder, H.: An ozone climatology based on ozonesonde and satellite measurements, J. Geophys. Res., 103, 31 709–31 734, 1998. 4234, 4238
Goerss, J. and Jeffries, R.: Assimilation of synthetic tropical cyclone observations into the Navy Operational Global Atmospheric Prediction System, Wea. Forecasting, 9, 557–576, 1994. 4229
Goerss, J. and Phoebus, P.: The Navy's operational atmospheric analysis, Wea. Forecasting, 7, 232–249, 1992. 4229, 4236, 4239
Goerss, J., Hogan, T., Sashegyi, K., Holt, T., Rennick, M., Beeck, T., and Steinle, P.: Validation Test Report for the NAVDAS/NOGAPS System, NRL Technical Report, 27, 2003. 4230
Grant, W. B., Browell, E. V., Butler, C. F., Gibson, S. C., Kooi, S. A., and von der Gathen, P.: Estimation of Arctic polar vortex ozone loss during the winter of 1999–2000 using vortex-

averaged airborne differential absorption lidar ozone measurements referenced to N_2O isopleths, J. Geophys. Res, 108(D10), 4309, doi:10.1029/2002JD002668, 2003. 4241
Harshvardhan, Davies, R., Randall, D., and Corsetti, T.: A fast radiation parameterization for atmospheric circulation models, J. Geophys. Res., 92, 1009–1016, 1987. 4233, 4234
Hines, C. O.: Doppler-spread parameterization of gravity-wave momentum deposition in the middle atmosphere, 1, basic formulation, J. Atmos. Sol.-Terr. Phys., 59, 371–386, 1997.
Hogan, T. and Rosmond, T.: The description of the Navy Operational Global Atmospheric Prediction System's spectral forecast model, Mon. Wea. Rev., 119, 1186–1815, 1991. 4229
Hogan, T. F., Rosmond, T. E., and Gelaro, R.: The NOGAPS forecast model: a technical description, Naval Oceanographic and Atmospheric Research Laboratory Report No. 13, 219, December, 1991. 4229
James, P. M.: A climatology of ozone mini-holes over the Northern hemisphere, Int. J. of Climatol., 18, 1287–1303, 1998.
Jang, K. I., Zou, X., De Pondeca, M. S. F. U., Shapiro, M., Davis, C., and Krueger, A.: Incorporating TOMS ozone measurements into the prediction of the Washington, DC, winter storm during 24–25 January 2000, J. Appl. Meteorol., 42, 797–812, 2003. 4230
Kasahara, A.: Various vertical coordinate systems used for numerical weather prediction, Mon. Wea. Rev., 102, 509–522, 1974 (corrigendum, Mon. Wea. Rev., 103, 664, 1975).
Kim, Y.-J.: Representation of subgrid-scale orographic effects in a general circulation model, 1, impact on the dynamics of simulated January climate, J. Climate, 9, 2698–2717, 1996. 4235
Kim, Y.-J. and Arakawa, A.: Improvement of orographic gravity-wave parameterization using a mesoscale gravity-wave model, J. Atmos. Sci., 52, 1875–1902, 1995. 4235
Lahoz, W. A.: Predictive skill of the UKMO Unified Model in the lower stratosphere, Q. J. R. Meteorol. Soc., 125, 2205–2238, 1999. 4249
Lawrence, B. N.: Some aspects of the sensitivity of stratospheric climate simulation to model lid height, J. Geophys. Res., 102, 23 805–23 811, 1997.
Lin, S.-J. and Williamson, D.: A middle atmosphere extension of the Held-Suarez forcing and age-of-air trace for dynamical core inter-comparison, NASA Global Modeling and Assimilation Office, http://gmao.gsfc.nasa.gov/sci_research/fvdas/LinWilliamson.ps, 2000. 4235
Louis, J. F.: A parametric model of vertical eddy fluxes in the atmosphere, Boundary Layer Meteorol., 17, 187–202, 1979. 4233
Louis, J. F., Tiedtke, M., and Geleyn, J. F.: A short history of the operational PBL parameteri-

zation at ECMWF, ECMWF Workshop on Planetary Boundary Parameterizations, November 1981, 59–79, 1982. 4233

McCormack, J. P. and Hood, L. L.: The frequency and size of ozone “mini-hole” events at northern midlatitudes in February, Geophys. Res. Lett., 24, 1997. 4229

McCormack, J. P. and Siskind, D. E.: Simulations of the quasi-biennial oscillation and its effect on stratospheric H_2O, CH_4, and age of air with an interactive two-dimensional model, J. Geophys. Res., 107 (D22), 4625, doi:10.1029/2002JD002095, 2002. 4235, 4252

McLinden, C. A., Olsen, S. C., Hannegan, B., Wild, O., Prather, M. J., and Sundet, J.: Stratospheric ozone in 3-D models: A simple chemistry and the cross-tropopause flux, J. Geophys. Res., 105, 14 653–14 665, 2000. 4238, 4254

McPeters, R. D., Bhartia, P. K., Kreuger, A. J., et al.: Earth Probe Total Ozone Mapping Spectrometer (TOMS) Data Products Users Guide, NASA Technical Publication 1998-206985, 64, NASA Goddard Space Flight Center, Greenbelt, MD, USA, 1998. 4240

Newman, P. A., Lait, L. R., and Schoeberl, M. R.: The morphology and meteorology of southern hemisphere spring total ozone mini-holes, Geophys. Res. Lett., 15, 923–926, 1988.

Orsolini, Y., Cariolle, D., and Deque, M.: Ridge formation in the lower stratosphere and its influence on ozone transport: A general circulation model study during late January 1992, J. Geophys. Res., 100, 11 113–11 135, 1995.

Palmer, T. N., Shutts, G. J., and Swinbank, R.: Allevation of a systematic westerly bias in general circulation and numerical weather prediction models through an orographic gravity wave drag parameterization, Q. J. R. Meteorol. Soc., 112, 1001–1039, 1986. 4235

Pawson, S., Langematz, U., Radek, G., Schlese, U., and Strauch, P.: The Berlin troposphere-stratosphere-mesosphere GCM: Sensitivity to physical parameterizations, Q. J. R. Meteorol. Soc., 124, 1343–1371, 1998.

Pumphrey, H. C., Rind, D., Russell III, J. M., and Harries, J. E.: A preliminary zonal mean climatology of water vapor in the stratosphere and mesosphere, Adv. Space Res., 21, 1417–1420, 1998. 4234

Randel, W. J., Boville, B. A., Gille, J. C., Bailey, P. L., Massie, S. T., Kumer, J. B., Mergenthaler, J. L., and Roche, A. E.: Simulation of stratospheric N_2O in the NCAR CCM2: comparison with CLAES data and global budget analysis, J. Atmos. Sci., 51, 2834–2845, 1994. 4252

Randel, W. J., Fleming, E., Geller, M., et al.: SPARC intercomparison of middle atmosphere climatologies, World Meteorological Organization Technical Document No. 1142, WCRP-116, 96, December, 2002. 4236

ACPD

4, 4227–4284, 2004

Rasch, P. J. and Williamson, D. L.: Computational aspects of moisture transport in global models of the atmosphere, Q. J. R. Meteorol. Soc., 116, 1071–1090, 1990. 4237
Rood, R. B., Nielsen, E., Stolarski, R. S., Douglass, A. R., Kaye, J. A., and Allen, D. J.: Episodic total ozone minima and associated effects on heterogeneous chemistry and lower stratospheric transport, J. Geophys. Res., 97, 7979–7996, 1992.
Shepherd, T. G., Semeniuk, K., and Koshyk, J. N.: Sponge layer feedbacks in middle-atmosphere models, J. Geophys. Res., 101, 23 447–23 464, 1996.
Simmons, A. J. and Burridge, D. M.: An energy and angular momentum conserving vertical finite-difference scheme and hybrid vertical coordinates, Mon. Wea. Rev., 109, 758–766, 1981.
Simmons, A. J., Hoskins, B. J., and Burridge, D. M.: Stability of semi-implicit time scheme, Mon. Wea. Rev., 106, 405–412, 1978. 4233
Stajner, I., Riishojgaard, L. P., and Rood, R. B.: The GEOS ozone data assimilation system: Specification of error statistics, Q. J. R. Meteorol. Soc., 127, 1069–1094, 2001. 4237, 4244
Stajner, I., Winslow, N., Rood, R. B., and Pawson, S.: Monitoring of observation errors in the assimilation of satellite ozone data, J. Geophys. Res., 109, D06309, doi:10.1029/2003JD004118, 2004. 4240
Swinbank, R. and Ortland, D. A.: Compilation of wind data for the Upper Atmosphere Research Satellite (UARS) Reference Atmosphere Project, J. Geophys. Res., 108, D19, 4615, doi:10.1029/2002JD003135, 2003. 4236
Teitelbaum, H., Moustaoui, M., and Fromm, M.: Exploring polar stratospheric cloud and ozone minihole formation: The primary importance of synoptic-scale flow perturbations, J. Geophys. Res., 106, 28 173–28 188, 2001.
Teixeira, J. and Hogan, T.: Boundary layer clouds in a global atmospheric model: Simple cloud cover parameterization, J. Climate, 15, 1261–1276, 2002. 4233
Tiedtke, M.: The sensitivity of the time-scale flow to cumulus convection in the ECMWF model, Workshop on Large-Scale Numerical Models, 28 November-1 December 1983, European Centre for Medium-Range Weather Forecasts, 297–316, 1984. 4233
Thomason, L. W. and Taha, G.: SAGE III aerosol extinction measurements: Initial results, Geophys. Res. Lett., 30(12), 1631, doi:10.1029/2003GL017317, 2003. 4240
Trenberth, K. E. and Stepaniak, D. P.: A pathological problem with NCEP reanalyses in the stratosphere, J. Climate, 15, 690–695, 2002. 4234
Urban, J., Lautié, N., Le Flochmoën, E. et al.: The northern hemisphere stratospheric

ACPD
4, 4227–4284, 2004

vortex during the 2002–2003 winter: Subsidence, chlorine activation and ozone loss observed by the Odin Sub-Millimetre Radiometer, Geophys. Res. Lett., 31, L07103, doi:10.1029/2003GL019089, 2004. 4231

Webster, S., Brown, A. R., Cameron, D. R., and Jones, C. P.: Improvements to the representation of orography in the Met Office Unified Model, Q. J. R. Meteorol. Soc., 129, 1989–2010, 2003. 4233

World Meteorological Organization: Scientific Assessment of Ozone Depletion: 2002, Global Ozone Research and Monitoring Project-Report No. 47, 498, Geneva, 2003.

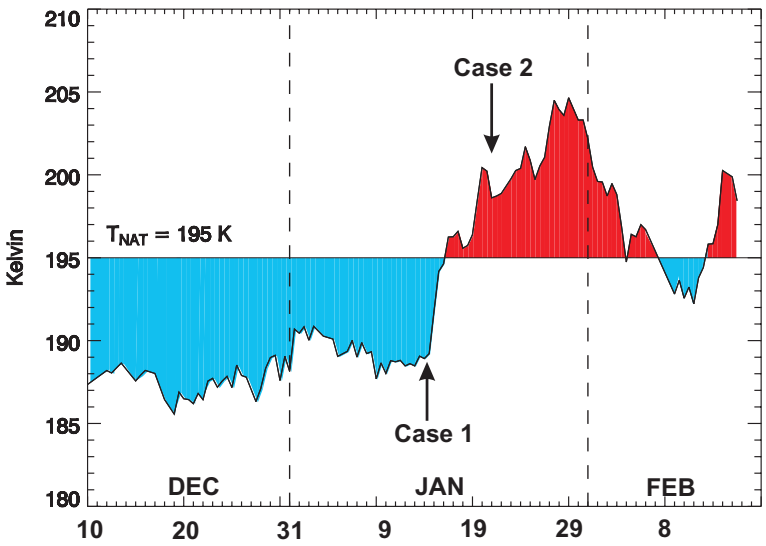

Fig. 1. Time series of minimum 30 hPa temperatures within 60°–90° N during the period 10 December 2002–18 February 2003 taken from operational NOGAPS analyses. Dotted vertical lines separate individual months. DC-8 flights on 14 January and 21 January are indicated as Case 1 and Case 2, respectively. Horizontal line denotes nominal 195 K PSC formation temperature threshold at 30 hPa.

ACPD
4, 4227–4284, 2004

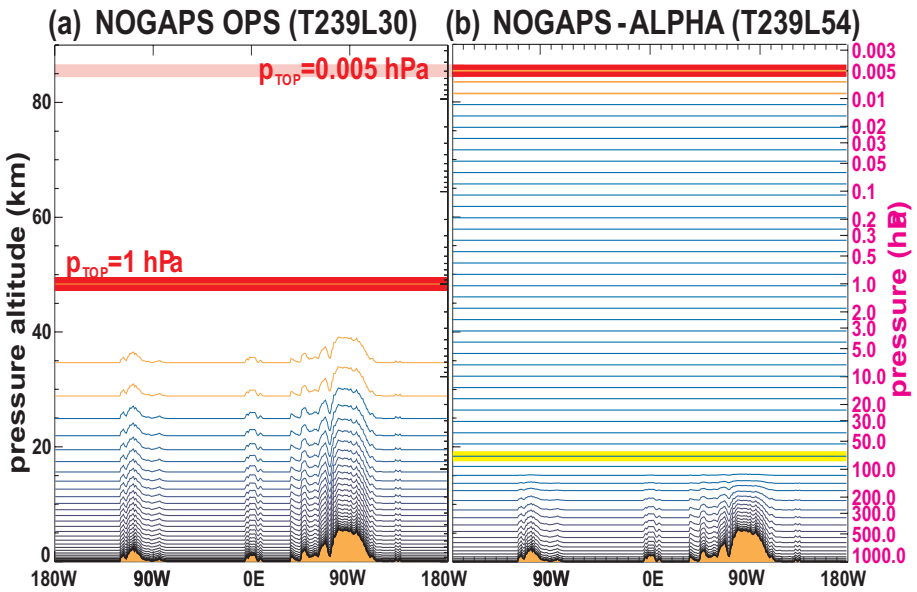

Fig. 2. NOGAPS vertical levels around 34.5° N latitude for: **(a)** operational 30-level (L30) model with p_{top}=1 hPa; **(b)** new NOGAPS-ALPHA 54-level (L54) model with p_{top}=0.005 hPa. Model layers near the top boundary where large numerical diffusion is applied are highlighted in orange.

ACPD
4, 4227–4284, 2004

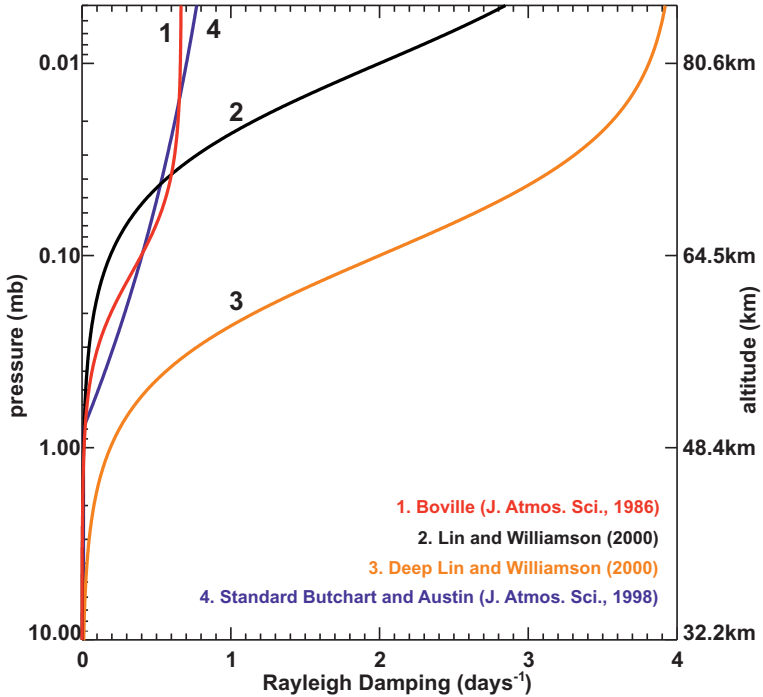

Fig. 3. Rayleigh friction profiles used in NOGAPS-ALPHA.

ACPD
4, 4227–4284, 2004

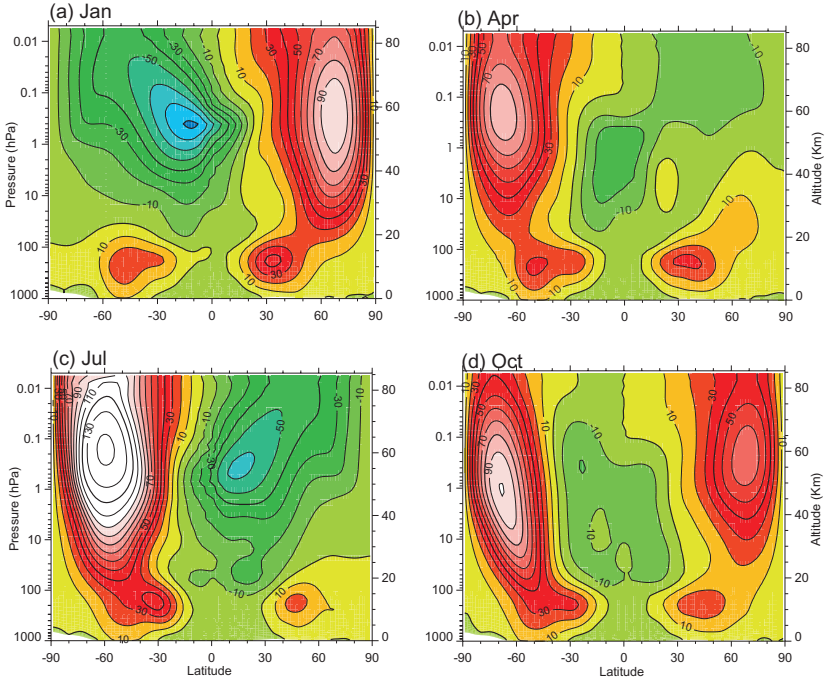

Fig. 4. Monthly zonal mean zonal winds from a 5-year T79L54 NOGAPS-ALPHA simulation for January, April, July, and October. Contours are drawn every 10 ms^{-1}. Westerly winds are shaded yellow to red, easterly winds are shaded green to blue.

ACPD
4, 4227–4284, 2004

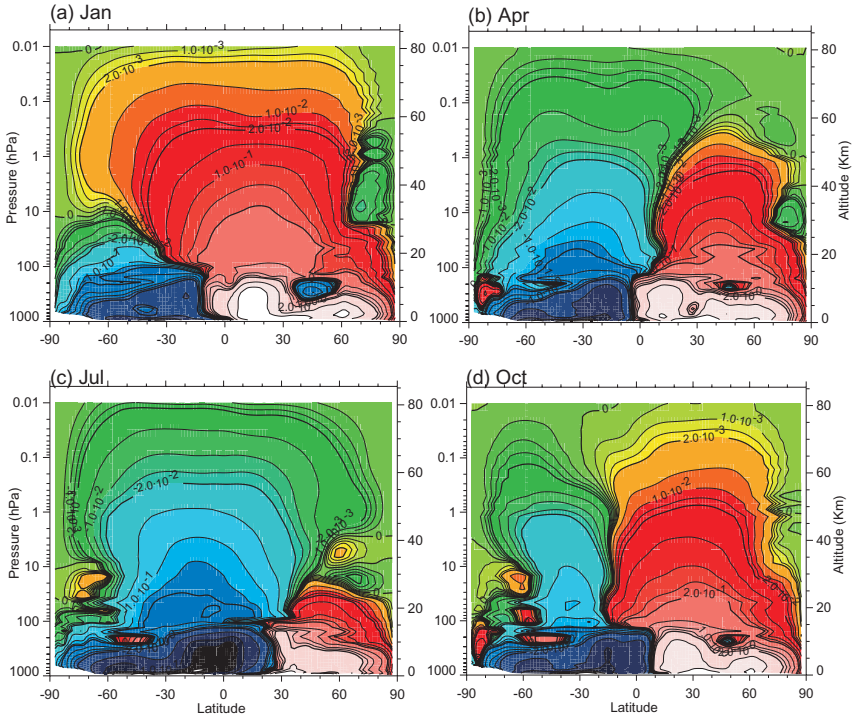

Fig. 5. Monthly mean meridional mass stream function from a 5-year T79L54 NOGAPS-ALPHA simulation for January, April, July, and October. Distance between contour lines is proportional to strength of mass flux. Clockwise circulation (positive contours) is shaded yellow to red, counter-clockwise circulation (negative contours) are shaded green to blue.

ACPD
4, 4227–4284, 2004

NOGAPS-ALPHA O_3 simulations during SOLVE2

J. P. McCormack et al.

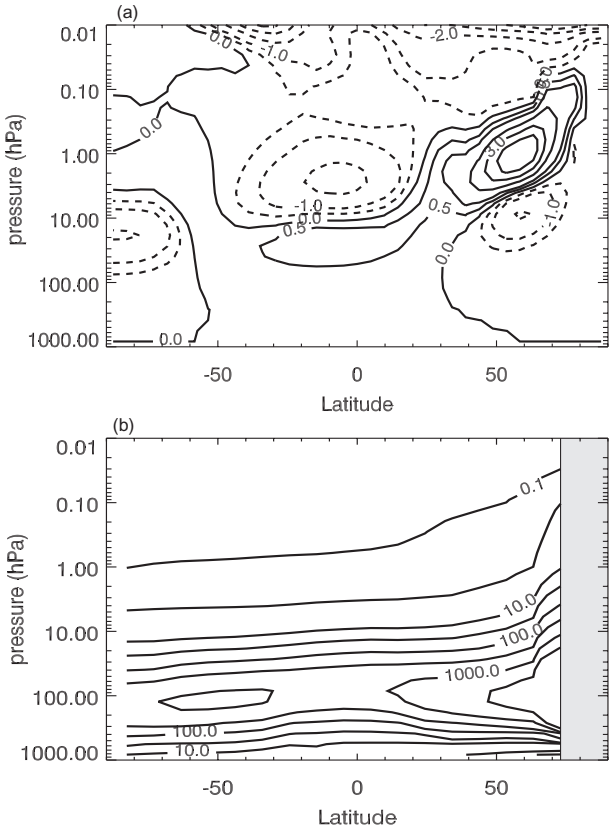

Fig. 6. Values of the **(a)** the net ozone mixing ratio tendency (ppmv month^{-1}) and **(b)** photochemical relaxation time (days) computed for mid-January conditions with the NRL CHEM2D model. Shaded region in (b) indicates polar night.

ACPD
4, 4227–4284, 2004




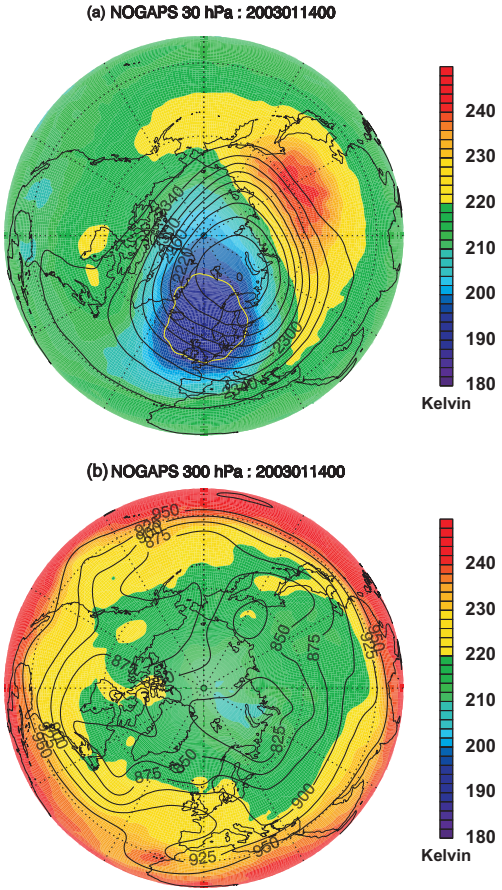

Fig. 7. Operational 1°×1° NOGAPS analyses of geopotential height in dam (solid contours) and temperature in Kelvin (colors) on 14 January 2003 for **(a)** 30 hPa and **(b)** 300 hPa. 30 hPa temperatures below 195 K are enclosed with a yellow contour. Polar projection extends to 20° N latitude.

ACPD

4, 4227–4284, 2004

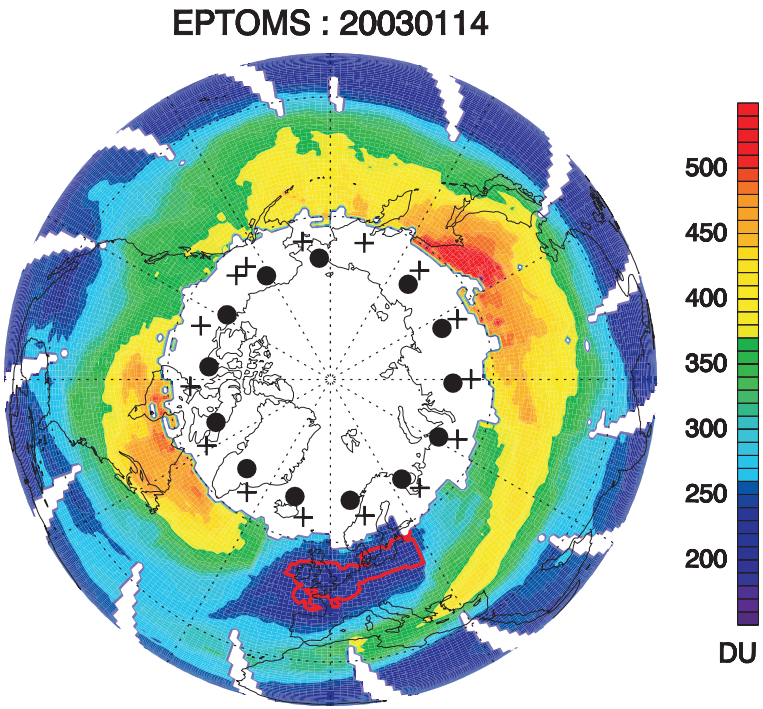

Fig. 8. EPTOMS total ozone on 14 January 2003. Polar projection extends to 20° N latitude. White areas denote missing data. Heavy red contour encloses area where total ozone column abundance is below 235 Dobson units (DU). Locations of POAM III (crosses) and SAGE III (circles) ozone profile measurements on this date are also indicated.

ACPD
4, 4227–4284, 2004

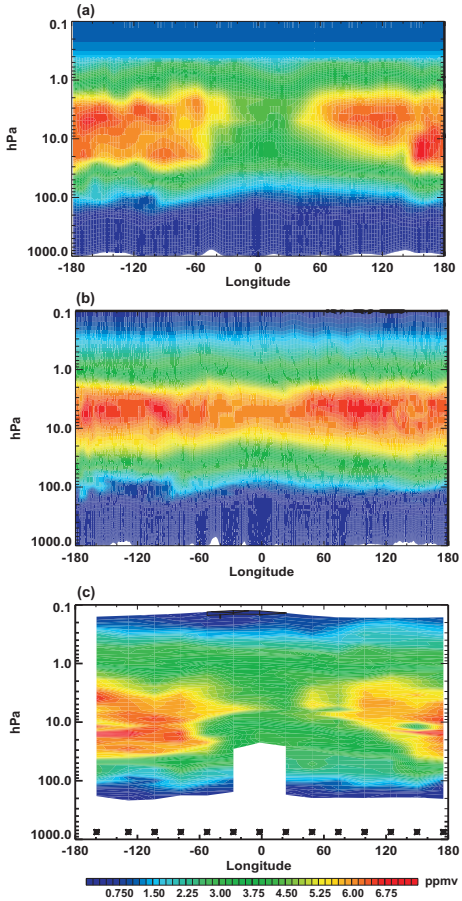

Fig. 9. **(a)** Ozone mixing ratios (ppmv) from the 11 January 2003 NASA GEOS4 analyses at 0 Z and 64.9° N latitude; **(b)** ozone mixing ratios from 11 January 2003 operational ECMWF analyses at 0 Z and 64.4° N; **(c)** POAM ozone mixing ratio measurements at 64.2° N on 11 January 2003, with asterisks indicating latitude of individual POAM profiles and white areas indicating missing data.

ACPD
4, 4227–4284, 2004

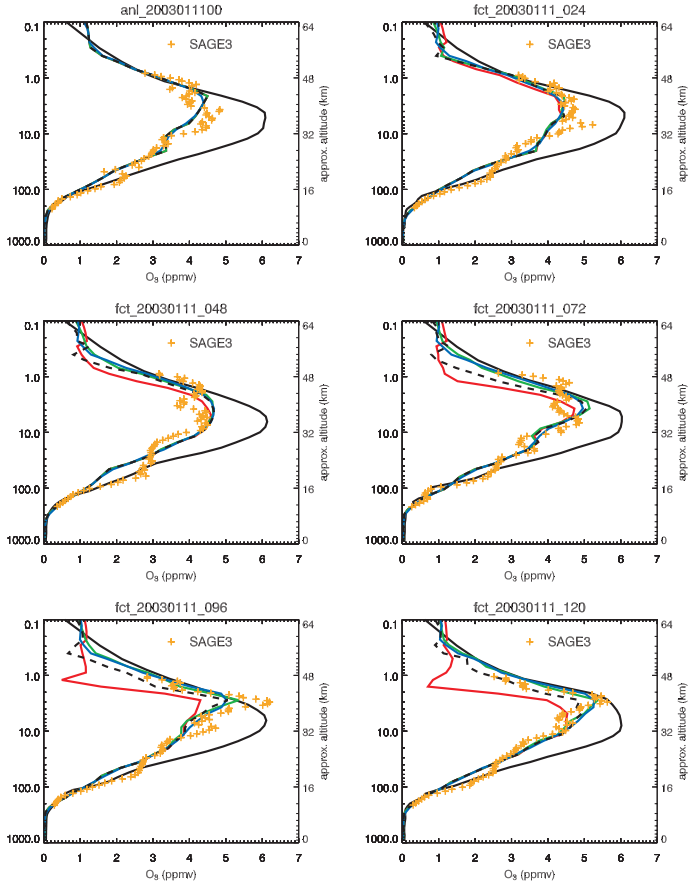

Fig. 10. NOGAPS-ALPHA ozone mixing ratio profiles over Kiruna, Sweden (68° N, 20° E) for a 5-day forecast initialized on 11 January 2003 using the CD86 (blue), LINOZ (red), and CHEM2D (green) photochemistry schemes. Passive ozone is plotted as a dashed black curve. Co-located SAGE III profiles are plotted as points. The solid black curve denotes the corresponding ECMWF ozone analysis and forecasts initialized on 11 January 2003.

ACPD
4, 4227–4284, 2004

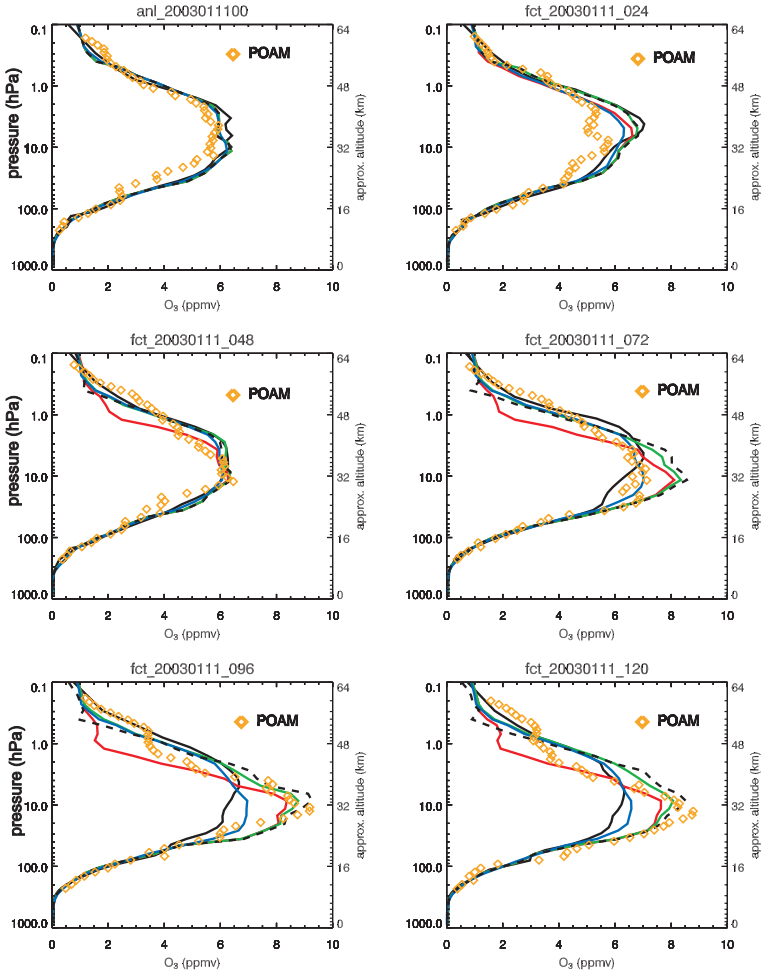

Fig. 11. As in Fig. 10, but now comparing NOGAPS-ALPHA ozone mixing ratio profiles at 65° N latitude, 135° E longitude with nearby POAM III ozone profiles (diamonds).

ACPD
4, 4227–4284, 2004

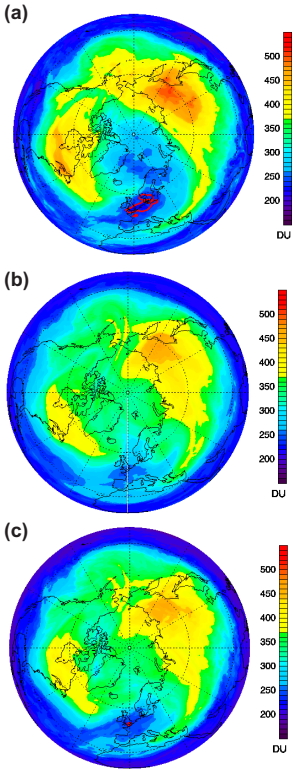

Fig. 12. **(a)** T239L54 NOGAPS-ALPHA total ozone at hour 96 of 5-day simulation initialized OZ 11 Jan 2003 with NASA GEOS4 ozone analyses and using the CHEM2D photochemistry scheme; **(b)** total ozone from corresponding 96-h operational T511L60 96-h ECMWF ozone forecast; **(c)** same as in (a) but using the CD86 photochemistry scheme and ECMWF ozone initialization. Red contour encloses region of total ozone <235 DU.

ACPD

4, 4227–4284, 2004

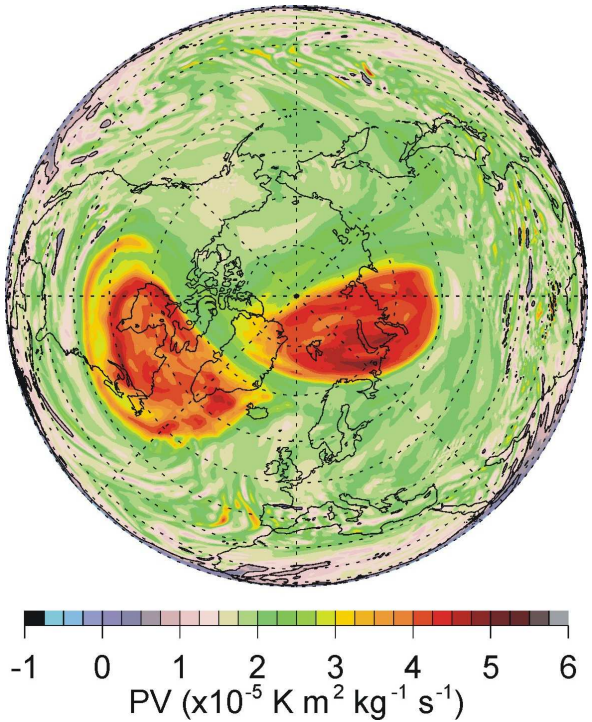

Fig. 13. EPV on the 460 K isentropic surface computed from ECMWF T511L60 operational analysis on 21 January 2003 at 18 Z.

ACPD
4, 4227–4284, 2004

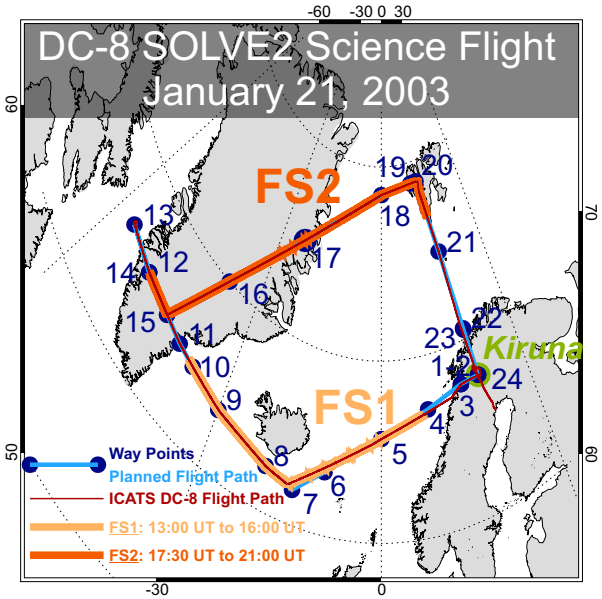

Fig. 14. Flight track of NASA DC-8 SOLVE2 science flight on 21 January 2003. Light blue curve shows planned flight track, with planned way points numbered with dark blue circles. Actual flight track, from the on-board Information Collection and Transmission System (ICATS), is plotted in dark red. Note that this DC-8 flight ends at a point southeast of Kiruna, due to a diverted landing in Lulea due to icy runway conditions at Kiruna airport. Two flight segments chosen for further analysis are shown in light orange and light red, corresponding to flight times shown in the bottom-left of the plot.

ACPD
4, 4227–4284, 2004

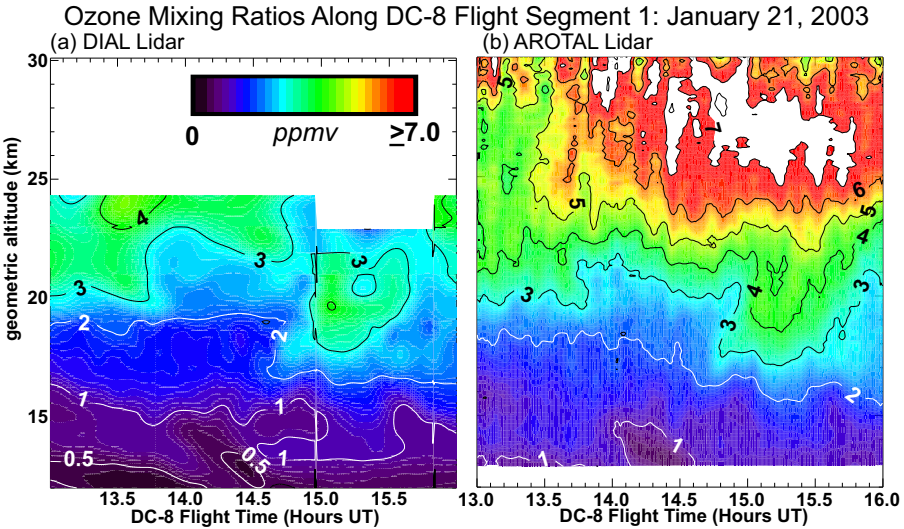

Fig. 15. Ozone mixing ratios (ppmv) as a function of geometric altitude along DC-8 flight segment 1 (FS-1) as measured by **(a)** DIAL lidar and **(b)** AROTAL lidar on 21 January 2003. The AROTAL values were smoothed along the time axis using a 9-point running average to reduce noisiness at upper levels caused by acquisition of data in sunlight. Color scale is 0–7 ppmv: values >7 ppmv are shaded white for AROTAL. White regions for DIAL denote missing data.

ACPD
4, 4227–4284, 2004

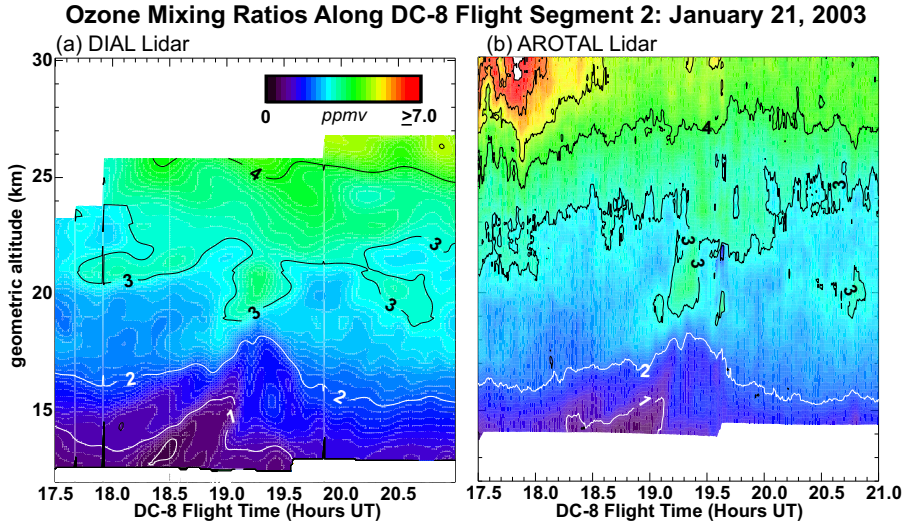

Fig. 16. Ozone mixing ratios (ppmv) as a function of geometric altitude along DC-8 flight segment 2 (FS-2) as measured by **(a)** DIAL lidar and **(b)** AROTAL lidar on 21 January 2003. AROTAL values were not smoothed here due to greater signal-to-noise provided by data acquisition in polar night. Color scale is 0–7 ppmv: values >7 ppmv are shaded white for AROTAL. White regions for DIAL denote missing data.

ACPD
4, 4227–4284, 2004

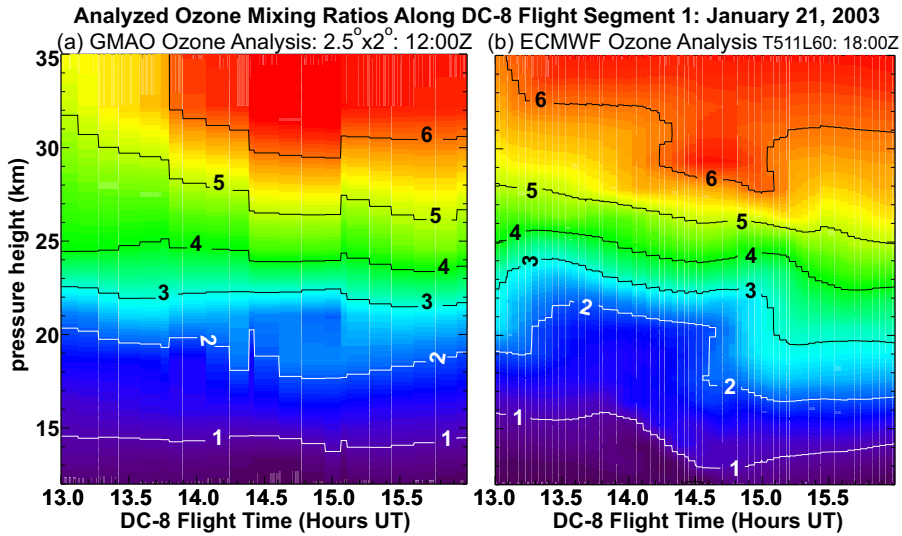

Fig. 17. Analysis ozone mixing ratios (ppmv) as a function of pressure altitude along the DC-8 flight segment 1 (FS-1) from **(a)** GEOS4 2.5°×2° analysis, and **(b)** operational ECMWF analysis fields from T511L60 model (on a reduced N256 grid). Both analyses are for 21 January 2003: GEOS4 is taken at 12 Z, ECMWF is taken at 18 Z. Altitude range is extended to ~35 km to account for differences in pressure and geometric altitudes.

ACPD
4, 4227–4284, 2004

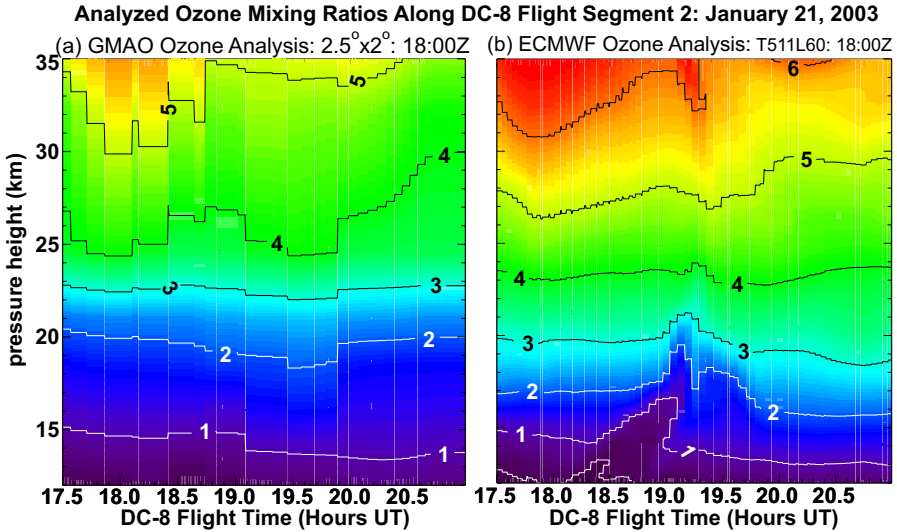

Fig. 18. Analysis ozone mixing ratios (ppmv) as a function of pressure altitude along the DC-8 flight segment 2 (FS-2) from **(a)** GEOS4 2.5°×2° analysis, and **(b)** operational ECMWF analysis fields from T511L60 model (on a reduced N256 grid). Both analyses here are for 21 January 2003 at 18 Z. Altitude range is extended to ~35 km to account for differences in pressure and geometric altitudes.

ACPD
4, 4227–4284, 2004

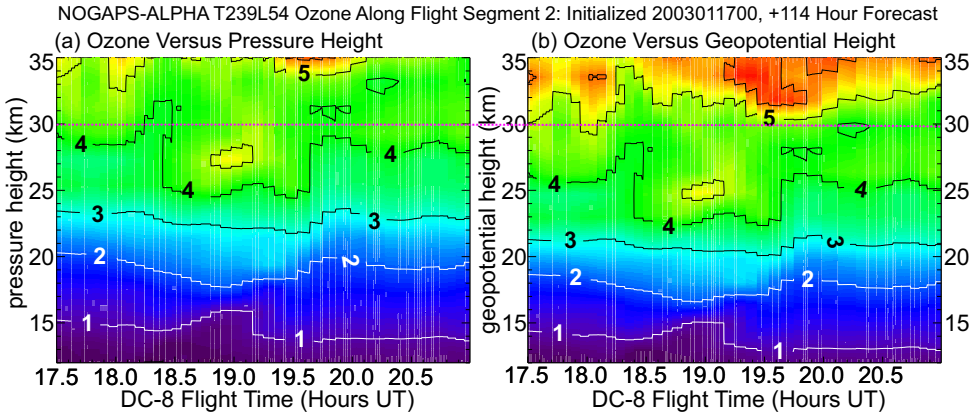

Fig. 19. NOGAPS-ALPHA T239L54 +114 h hindcast ozone for 21 January 2003 at 18 Z, plotted along DC-8 flight segment 2 as a function of **(a)** pressure height, and **(b)** geopotential height. The latter is more directly comparable to the geometric heights used for the lidar ozone profiles in Fig. 16: dotted pink line shows 30 km upper boundary of lidar plot.

ACPD
4, 4227–4284, 2004

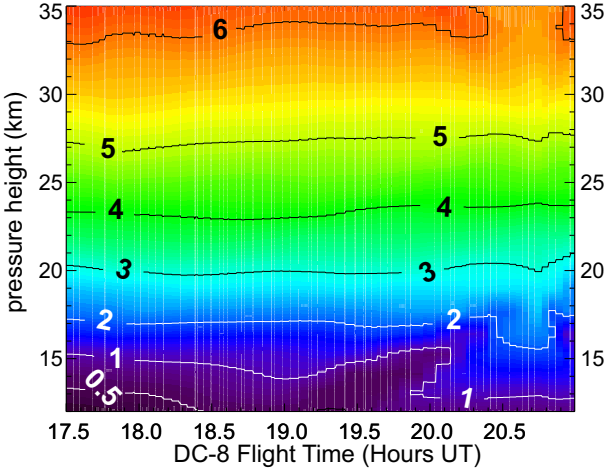

Fig. 20. Archived ECMWF T511L60 114-h operationally forecast ozone for 21 January 2003 at 18 Z, plotted along DC-8 flight segment 2 as a function of pressure height.

ACPD
4, 4227–4284, 2004

NOGAPS-ALPHA O_3 simulations during SOLVE2

J. P. McCormack et al.

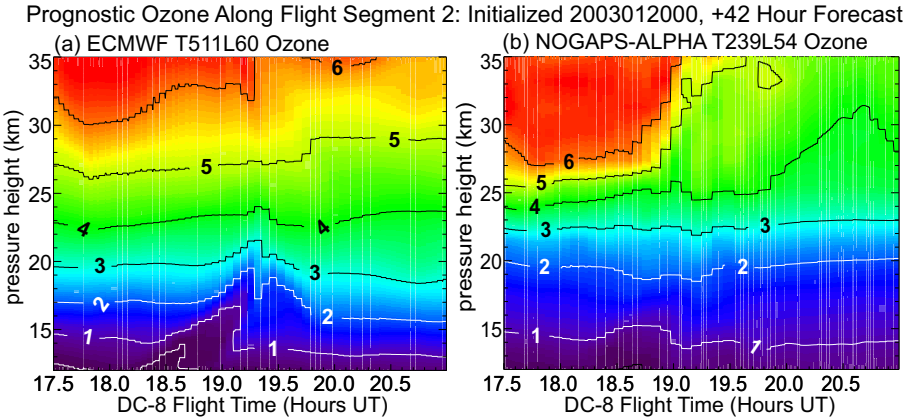

Fig. 21. (a) Archived ECMWF T511L60 42-h operationally forecast ozone for 21 January 2003 at 18 Z, plotted along DC-8 flight segment 2 as a function of pressure height. **(b)** NOGAPS-ALPHA T239L54 42-h hindcast ozone along flight segment 2.

ACPD
4, 4227–4284, 2004

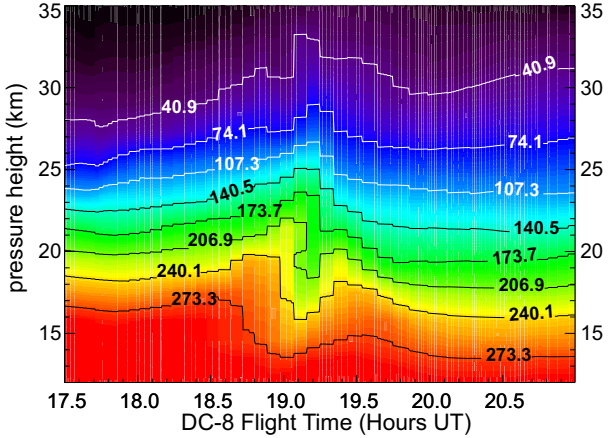

Fig. 22. NOGAPS-ALPHA T239L54 42-h hindcast of psuedo-N_2O mixing ratios (ppbv) initialized from 2-D climatology, valid for 21 January 2003 at 18 Z and projected along flight segment 2.

ACPD
4, 4227–4284, 2004

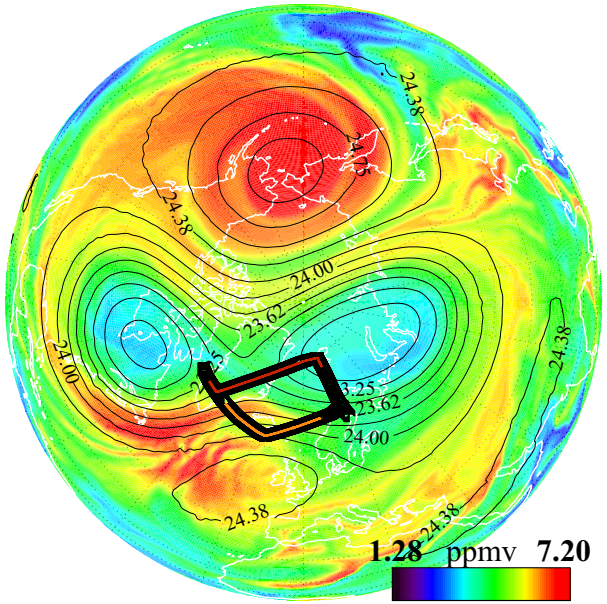

Fig. 23. NOGAPS-ALPHA T239L54 42-h hindcast of O_3 mixing ratios (ppmv) at 26.7 hPa, valid for 21 January 2003 at 18 Z. The DC-8 flight and flight segments (FS-1, FS-2) from Fig. 14 are overplotted. Contours are geopotential heights in kilometers.

ACPD
4, 4227–4284, 2004